

Calibration of Ordinal Regression Networks

Daehwan Kim¹ Haejun Chung^{1,2,3} Ikbeom Jang^{4,5,6}

Abstract

Recent studies have shown that deep neural networks are not well-calibrated and often produce over-confident predictions. The miscalibration issue primarily stems from using cross-entropy in classifications, which aims to align predicted softmax probabilities with one-hot labels. In ordinal regression tasks, this problem is compounded by an additional challenge: the expectation that softmax probabilities should exhibit unimodal distribution is not met with cross-entropy. The ordinal regression literature has focused on learning orders and overlooked calibration. To address both issues, we propose a novel loss function that introduces ordinal-aware calibration, ensuring that prediction confidence adheres to ordinal relationships between classes. It incorporates soft ordinal encoding and ordinal-aware regularization to enforce both calibration and unimodality. Extensive experiments across four popular ordinal regression benchmarks demonstrate that our approach achieves state-of-the-art calibration without compromising classification accuracy.

1. Introduction

Recent advances in ordinal regression tasks (e.g., medical diagnosis and rating assessments) have primarily focused on improving accuracy, often disregarding *calibration*. In high-risk applications, deep neural networks (DNNs) must not only be accurate but also provide reliable confidence estimates that reflect the true likelihood of correctness (Guo et al., 2017). Although ordinal regression inherently involves a natural ordering of classes, existing approaches

¹Department of Artificial Intelligence Semiconductor Engineering, Hanyang University, Seoul, Republic of Korea ²Department of Artificial Intelligence, Hanyang University, Seoul, Republic of Korea ³Department of Electronic Engineering, Hanyang University, Seoul, Republic of Korea ⁴Division of Computer Engineering, Hankuk University of Foreign Studies, Yongin, Republic of Korea ⁵Division of AI Data Convergence, Hankuk University of Foreign Studies, Yongin, Republic of Korea ⁶Division of Language & AI, Hankuk University of Foreign Studies, Yongin, Republic of Korea. Correspondence to: Haejung Chung <haejun@hanyang.ac.kr>, Ikbeom Jang <ijang@hufs.ac.kr>.

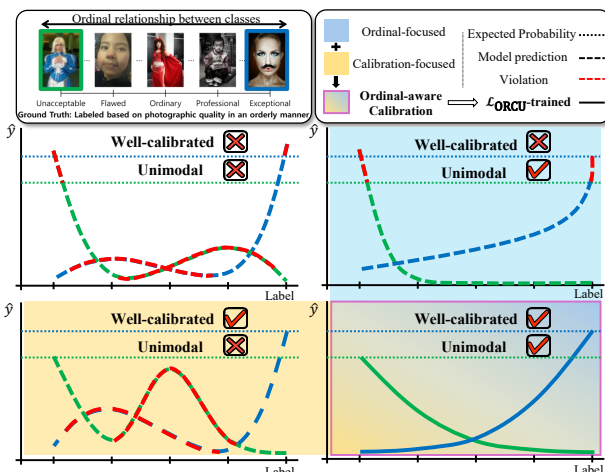


Figure 1. Comparison of probability distributions for model predictions trained with loss functions targeting different objectives in ordinal classification. Top left: Model trained without any calibration or unimodality constraints. Top right: Ordinal-focused loss, producing unimodal but uncalibrated predictions. Bottom left: Calibration-focused loss, yielding calibrated but non-unimodal predictions. Bottom right: Proposed $\mathcal{L}_{\text{ORCU}}$, achieving both calibrated and unimodal predictions.

have neglected mainly the joint consideration of calibration and ordinal relationships, leaving a critical gap in addressing these interdependent aspects effectively. Such miscalibration poses serious risks in domains where precision and reliability are essential. To the best of our knowledge, this is the first study to explicitly address both calibration and ordinality in ordinal regression.

Ordinal regression, also termed ordinal classification, involves a natural ordering between class labels as opposed to nominal classification. Existing approaches, including regression-based (Fu & Huang, 2008; Pan et al., 2018; Yang et al., 2018; Li et al., 2019), classification-based (Liu et al., 2020; Polat et al., 2022a; Vargas et al., 2022), and ranking-based approaches (Niu et al., 2016; Chen et al., 2017; Cao et al., 2020; Shi et al., 2023), effectively model this inherent ordinal structure. However, these approaches often overlook calibration, leading to unreliable confidence estimates. This shortfall is particularly problematic in sensitive domains (Jiang et al., 2012; Neumann et al., 2018; Moon et al., 2020; Kompa et al., 2021), where trustworthy confidence levels

must accompany ordered predictions.

Calibration ensures that the predicted probability of a model aligns with the true likelihood of correctness, formally requiring $P(Y = y \mid \hat{P} = p) = p$, where \hat{P} is the model’s predicted confidence. In high-stakes applications, such as medical diagnosis and autonomous driving, low-confidence predictions can prompt further verification processes, thereby ensuring safety and reliability. For tasks with ordinal labels, calibration is particularly crucial to ensure that confidence values accurately reflect the reliability of predictions, facilitating more reliable decision-making.

Beyond calibration, unimodality in output distributions is vital for robust ordinal classification. Under the assumption that the true conditional distribution $P_{Y|X}$ is *unimodal* (Dey et al., 2024), there exists a class c_m for which probabilities increase monotonically up to c_m and decrease thereafter. Violating this assumption can cause contradictions, such as predicting c_1 as most probable while giving c_4 the second highest probability. Ensuring unimodality prevents such irrational predictions by guaranteeing that c_m corresponds to the highest predicted probability. Enforcing unimodality thus strengthens the consistency and credibility of ordinal classification models (Li et al., 2022; Vargas et al., 2022).

Figure 1 illustrates how focusing solely on calibration or ordinality can yield miscalibrated predictions or outputs that ignore intrinsic label ordering. This emphasizes the need for a loss function simultaneously targeting both calibration and unimodality, ensuring well-calibrated and orderly probability distributions in ordinal classification tasks.

To address these dual challenges, we propose *Ordinal Regression loss for Calibration and Unimodality* (ORCU), a novel loss function that jointly enforces calibration and ordinal relationships. ORCU explicitly encodes the ordering of classes and incorporates an ordinal-aware regularization term to align predicted probabilities with the inherent class order while preserving reliable confidence estimates. By concurrently addressing calibration and ordinality, ORCU produces accurate and credible predictions, making it well-suited for critical applications demanding both precision and trustworthiness.

Contributions: We make the following key contributions:

- We propose ORCU, a loss function that improves calibration and unimodality within a unified framework for ordinal regression. It integrates soft encoding with regularization that enforces ordinal-aware conditions, ensuring that predicted probabilities align with ordinal relationships while improving reliable confidence estimates.
- We provide a comprehensive analysis demonstrating how ORCU effectively balances the trade-off between

well-calibrated confidence estimates and accurate predictions, addressing limitations in existing methods that focused only on either calibration or ordinal structure.

- Our approach sets a new benchmark for reliable ordinal classification, advancing the state-of-the-art and guiding future research on trustworthy models for ordinal tasks.

2. Related Work

2.1. Ordinal Regression

Predicting a target value involves mapping an input $x \in \mathcal{X}$ to a target $y \in \mathcal{Y}$ via a function $\mathcal{M} : \mathcal{X} \rightarrow \mathcal{Y}$ such that $\mathcal{M}(x) = y$. Nominal and ordinal predictions are two typical cases. Nominal tasks treat labels in \mathcal{Y} as discrete and unordered, handling each label independently. In contrast, ordinal tasks involve a sequential structure within \mathcal{Y} , represented as $y_1 \prec y_2 \prec \dots \prec y_C$, where \prec denotes an ordinal relationship (e.g., y_i is smaller than y_{i+1}). This structure requires specialized methods, collectively termed ordinal regression. Approaches to ordinal regression can be broadly divided into three: traditional regression, classification-based, and ranking-based methods. Traditional regression methods (Fu & Huang, 2008; Pan et al., 2018; Yang et al., 2018; Li et al., 2019) treat ordinal labels y as continuous variables, applying ℓ_1 -loss or ℓ_2 -loss to predict a scalar that reflects label ordering. Classification-based methods (Liu et al., 2020; Polat et al., 2022a; Vargas et al., 2022) discretize the target space into bins, treating each bin as a distinct class $y \in \{1, 2, \dots, C\}$ and directly predicting the class. Ranking-based methods (Niu et al., 2016; Chen et al., 2017; Cao et al., 2020; Shi et al., 2023) decompose the task into $C - 1$ binary classifiers, each represented by $\mathcal{M}_c : \mathcal{X} \rightarrow \{0, 1\}$ for $c = 1, \dots, C - 1$, where each \mathcal{M}_c determines whether y exceeds a class index c , thereby capturing ordinal relationships. In this work, we focus on classification-based ordinal regression, as it effectively captures ordinal relationships and supports calibration, which is intractable in regression or ranking-based methods due to their indirect probabilistic outputs (Song et al., 2019; Vaicenavicius et al., 2019).

2.2. Loss functions for ordinal regression

The limitations of Cross-Entropy (CE) loss in capturing ordinal relationships have led to several modified approaches in classification-based ordinal regression. Soft ORDinal (SORD) encoding (Diaz & Marathe, 2019) adjusts label distributions by employing soft labels to reflect class proximity, yielding smoother and more order-aware predictions. Class Distance Weighted Cross-Entropy (CDW-CE) (Polat et al., 2022a) retains traditional label structure but introduces a

distance-based penalty, guiding predictions closer to the true class and aligning with the ordinal structure. CO2 (Albuquerque et al., 2021) extends CE with a regularization term enforcing unimodality, ensuring predicted probabilities decrease smoothly with increasing distance from the true label. Finally, Probabilistic Ordinal Embeddings (POE) (Li et al., 2021) incorporate both a regularization term and architectural modifications, representing each label as a probability distribution to jointly model uncertainty and ordinal relationships. However, none of these approaches explicitly address calibration, leaving the reliability of their confidence estimates unexamined—a critical gap in applications requiring both accuracy and dependable confidence.

2.3. Regularization-based loss functions for calibration

Calibration, which aligns predicted confidence with actual accuracy, is critical in ordinal, multi-class classification tasks and can be approached through either post-hoc (Platt et al., 1999; Guo et al., 2017; Tomani et al., 2021; 2022) or regularization-based methods. Post-hoc methods often leave non-maximal classes uncalibrated, whereas regularization-based methods address this by calibrating the entire distribution during training (Hebbalaguppe et al., 2022). Several regularization-based approaches have been proposed to improve calibration without relying on post hoc adjustments. Label Smoothing (LS) (Szegedy et al., 2016) is a foundational technique that softens the sharpness of one-hot label distributions to mitigate overconfidence. Sample-dependent Focal Loss (FLSD) (Mukhoti et al., 2020) builds upon this by focusing calibration improvements on harder-to-classify examples. Margin-based Label Smoothing (MbLS) (Liu et al., 2022) selectively smooths predictions based on the margin between predicted logits and true labels, while Multi-class Difference in Confidence and Accuracy (MDCA) (Hebbalaguppe et al., 2022) extends this margin adjustment across the predicted distribution. Adaptive and Conditional Label Smoothing (ACLS) (Park et al., 2023) dynamically adjusts the level of smoothing, applying stronger smoothing to miscalibrated predictions while preserving confidence for well-calibrated cases. While regularization-based calibration methods are well-established, their application in ordinal tasks remains underexplored despite the crucial role of reliable confidence estimates in these settings.

3. Unified Ordinal Loss for Both Calibration and Unimodality

In ordinal classification tasks, capturing class ordering is essential for achieving both accuracy and reliable confidence estimates. However, existing methods often struggle with calibration and fail to leverage ordinal relationships effectively. We propose a novel loss function that explicitly encodes ordinal relationships and enforces unimodality

through a regularization term, enabling accurate and well-calibrated predictions for reliable decision-making.

3.1. Cross-Entropy Limitations in Ordinal Tasks

Let N denote the total number of samples and C represent the number of classes. For the n -th sample, where $n = 1, \dots, N$, let $y_n \in \{1, \dots, C\}$ denote the true class label. The CE loss is defined as $\mathcal{L}_{\text{CE}} = -\sum_{n=1}^N \sum_{k=1}^C y_{n,k} \log(\hat{y}_{n,k})$, where $y_{n,k}$ and $\hat{y}_{n,k}$ are the k -th components of the one-hot encoded true label $\mathbf{y}_n \in \mathbb{R}^C$ and the predicted probability vector $\hat{\mathbf{y}}_n = \text{softmax}(\mathbf{z}_n) \in \mathbb{R}^C$, respectively. Here, $\mathbf{z}_n = [z_{n,1}, \dots, z_{n,C}] \in \mathbb{R}^C$ denotes the logit vector for the n -th sample, with each $z_{n,k}$ representing the raw score for class k . The gradient of \mathcal{L}_{CE} with respect to each class logit is given as $\frac{\partial \mathcal{L}_{\text{CE}}}{\partial z_{n,k}} = \hat{y}_{n,k} - y_{n,k}$. Because only the target class term enters the loss directly, this formulation ignores relationships to neighboring classes. In ordinal settings, where the conditional distribution of class probabilities is expected to decrease around the true label, optimizing CE often produces an overemphasis on the true label. Consequently, it fails to distribute probabilities across adjacent classes in a manner reflective of their ordinal proximity, which can lead to unreliable predictions in critical applications.

3.2. Ordinal Soft Encoding

The fundamental limitation of CE in ordinal tasks stems from its reliance on the one-hot encoding of the true label. This encoding aligns $\hat{\mathbf{y}}_n$ with a sharply peaked true distribution \mathbf{y}_n (i.e., $y_{n,k} \approx 1$ for $k = y_n$), allowing only the target label to influence the entropy calculation and thus neglecting ordinal relationships. Furthermore, because the softmax function never outputs exactly 1, the model is repeatedly driven to increase the logit of the target class, leading to overconfident predictions. To address these issues, we adopt SORD encoding (Diaz & Marathe, 2019), which replaces one-hot encoding with a soft encoding that distributes values across classes based on inter-class distances, thereby mitigating overconfidence and capturing the ordinal structure among labels.

In this method, the true label y_n is represented as a soft-encoded vector $\mathbf{y}'_n \in \mathbb{R}^C$, where the k -th element $y'_{n,k}$ is defined as $y'_{n,k} = \frac{e^{-\phi(y_n, r_k)}}{\sum_{j=1}^C e^{-\phi(y_n, r_j)}}$ for $k = 1, \dots, C$, with $\phi(y_n, r_k)$ representing a distance metric that imposes a penalty based on the deviation between the true label y_n and each class r_k . Because $y'_{n,k} \in [0, 1]$ and $\sum_{k=1}^C y'_{n,k} = 1$, \mathbf{y}'_n forms a probability distribution that generalizes the one-hot encoded vector \mathbf{y}_n , effectively capturing ordinal relationships and reducing overconfidence by alleviating the drive to increase $z_{n,k}$ excessively to push the output probability $\hat{y}_{n,k}$ toward 1.

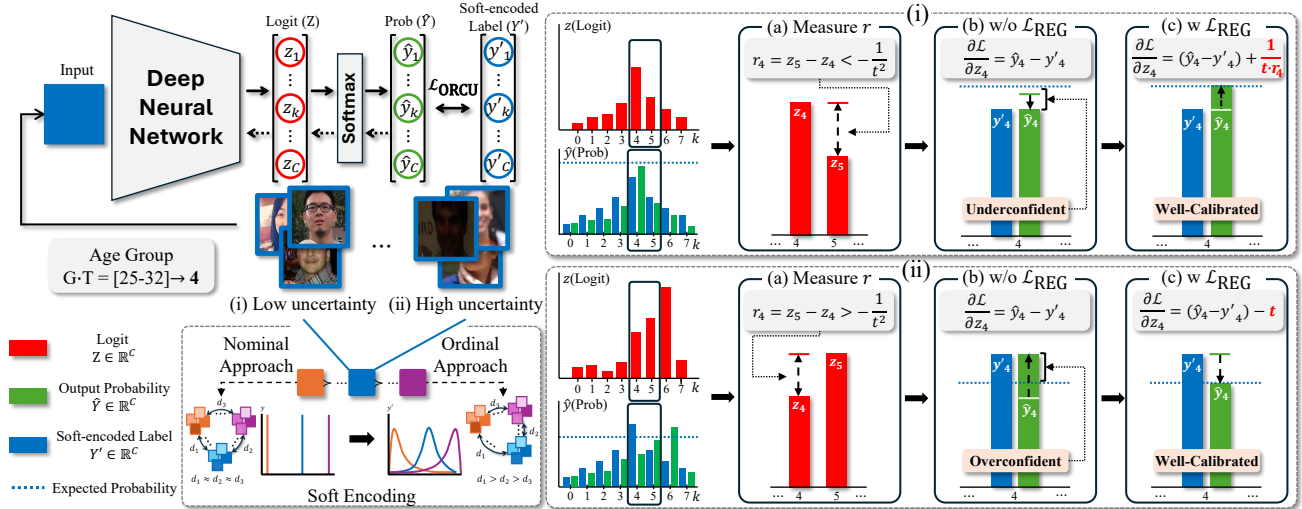


Figure 2. Illustration of ORCU’s impact on calibration and unimodality in ordinal classification using the Adience dataset (8 ordinal age classes). The figure demonstrates how \mathcal{L}_{REG} adjusts logits based on unimodality and uncertainty for (i) a low-uncertainty sample and (ii) a high-uncertainty sample, both for the case $k \geq y_n$. Each case includes: (a) computation of r , the logit difference quantifying uncertainty and unimodality; (b) updates without the ordinal-aware regularization, leading to inadequate calibration; and (c) updates with regularization, incorporating input-specific characteristics for improved calibration. See Section 3.4 and Table 1 for details.

The Soft-Encoded Cross-Entropy (SCE) loss, based on the soft label vector $y'_{n,k}$, is then defined as:

$$\mathcal{L}_{\text{SCE}} = - \sum_{n=1}^N \sum_{k=1}^C y'_{n,k} \log(\hat{y}_{n,k}). \quad (1)$$

Similar to the optimization properties of standard CE, the gradient of \mathcal{L}_{SCE} with respect to $z_{n,k}$, given by $\frac{\partial \mathcal{L}_{\text{SCE}}}{\partial z_{n,k}} = \hat{y}_{n,k} - y'_{n,k}$, aligns \hat{y}_n with y'_n , which represents an explicitly encoded approximation of the expected conditional distribution of class probabilities, thereby capturing ordinal relationships and mitigating overconfidence.

3.3. Ordinal-Aware Regularization

\mathcal{L}_{SCE} captures ordinal relationships and mitigates overconfidence by applying soft encoding based on inter-class deviations. However, this explicit adjustment can constrain the model’s flexibility in representing diverse data distributions, potentially confining output probabilities within a limited range and leading to underconfident predictions.

To address the miscalibration that may arise from explicitly preserving ordinal relationships, we incorporate an ordinal-aware regularization term (Belharbi et al., 2019) into \mathcal{L}_{SCE} . Unlike conventional calibration methods, which typically focus on the highest probability class (Park et al., 2023), our approach leverages a regularization strategy that explicitly preserves the ordinal structure inherent in the labels. Specifically, we partition the label space into regions $k < y_n$ and $k \geq y_n$, adjusting logits relative to y_n within each region. This structured approach enforces unimodality around y_n ,

thereby improving calibration while preserving the task’s essential ordinal relationships.

The regularization term is defined as follows:

$$\mathcal{L}_{\text{REG}} = \sum_{n=1}^N \sum_{k=1}^{C-1} \begin{cases} \hat{I}(z_{n,k} - z_{n,k+1}), & \text{if } k < y_n, \\ \hat{I}(z_{n,k+1} - z_{n,k}), & \text{if } k \geq y_n, \end{cases} \quad (2)$$

where $\hat{I}(r) = \begin{cases} -\frac{1}{t} \log(-r), & \text{if } r \leq -\frac{1}{t^2}, \\ tr - \frac{1}{t} \log\left(\frac{1}{t^2}\right) + \frac{1}{t}, & \text{otherwise.} \end{cases}$ This

penalty function, \hat{I} , applies a linear penalty for violations of unimodality while utilizing a log-barrier-based penalty with a logarithmic form within the satisfied region. The logarithmic nature of the log-barrier function enforces strong corrections as the difference r (where $r = z_{n,k} - z_{n,k+1}$ for $k < y_n$ and $r = z_{n,k+1} - z_{n,k}$ for $k \geq y_n$) approaches the boundary value $-1/t^2$, indicating a high-risk violation requiring a strong penalty. This structured adjustment ensures unimodality and improves calibration (see Section 3.4 for further details). The temperature parameter t modulates the tolerance and magnitude of these corrections (Table 1). The final ORCU loss function is defined as:

$$\mathcal{L}_{\text{ORCU}} = \mathcal{L}_{\text{SCE}} + \mathcal{L}_{\text{REG}}. \quad (3)$$

By combining \mathcal{L}_{SCE} and \mathcal{L}_{REG} , $\mathcal{L}_{\text{ORCU}}$ promotes both well-calibrated predictions and unimodality in the model’s output distribution.

Table 1. Gradient analysis of our loss function, showing gradients w.r.t. logits for $k < y_n$ and $k \geq y_n$. $\hat{y}_{n,k}$ and $y'_{n,k}$ are the k -th elements of the predicted probability vector $\hat{\mathbf{y}}_n$ and the soft-encoded target vector \mathbf{y}'_n for the n -th sample. t controls the regularization strength. Note that $\frac{\partial \mathcal{L}_{\text{ORCU}}}{\partial z_k} = \frac{\partial \mathcal{L}_{\text{SCE}}}{\partial z_k} + \frac{\partial \mathcal{L}_{\text{REG}}}{\partial z_k}$.

	$k < y_n$ ($r = z_{n,k} - z_{n,k+1}$)		$k \geq y_n$ ($r = z_{n,k+1} - z_{n,k}$)	
	$r \leq -\frac{1}{t^2}$	$r > -\frac{1}{t^2}$	$r \leq -\frac{1}{t^2}$	$r > -\frac{1}{t^2}$
(a) $\frac{\partial \mathcal{L}_{\text{SCE}}}{\partial z_{n,k}}$		$\hat{y}_{n,k} - y'_{n,k}$		
(b) $\frac{\partial \mathcal{L}_{\text{REG}}}{\partial z_{n,k}}$	$-\frac{1}{t-r}$	t	$\frac{1}{t-r}$	$-t$
(c) $\frac{\partial \mathcal{L}_{\text{ORCU}}}{\partial z_{n,k}}$	$(\hat{y}_{n,k} - y'_{n,k}) - \frac{1}{t-r}$	$(\hat{y}_{n,k} - y'_{n,k}) + t$	$(\hat{y}_{n,k} - y'_{n,k}) + \frac{1}{t-r}$	$(\hat{y}_{n,k} - y'_{n,k}) - t$

3.4. Gradient Analysis: Enforcing Unimodality and Calibration

To clarify how $\mathcal{L}_{\text{ORCU}}$ promotes both calibration and unimodality, we analyze the gradient of its ordinal-aware regularization term, \mathcal{L}_{REG} , conditioned on ordinal label relationships. Anchored on the true label y_n , \mathcal{L}_{REG} partitions the label space, guiding logits to decrease as they move away from the target, thus preserving a consistent ordinal relationship. Specifically, for $k < y_n$, z_k is guided to be lower than neighboring logits, whereas, for $k \geq y_n$, z_k is encouraged to be higher. These conditions are enforced through the gradient update of $\mathcal{L}_{\text{ORCU}}$, which integrates \mathcal{L}_{SCE} and \mathcal{L}_{REG} , as $z_k \leftarrow z_k - \eta \frac{\partial \mathcal{L}_{\text{ORCU}}}{\partial z_k}$. As a result, the model outputs align with the ordinal structure and thereby achieve improved calibration.

The difference between neighboring logits, r , reflects both the degree of unimodality and the associated uncertainty in the predicted distribution. Deviations of the predicted distribution $\hat{P}_{Y|X}$ from the expected unimodal structure indicate increased uncertainty, while closer adherence suggests stronger alignment with the true conditional distribution and reduced uncertainty. Specifically, suppose $\hat{P}_{Y|X}$ fails to exhibit a unimodal distribution. In that case, the model’s output probabilities are misaligned with the expected ordinal structure, resulting in heightened uncertainty in the predictions. This interpretation of r allows the model to respond to varying levels of uncertainty and unimodality adaptively. The gradient behavior is analyzed across four cases: the label space is partitioned by the true label y_n and further segmented by r values, as shown in Table 1-(c).

In cases where $r \ll -1/t^2$ (see Figure 2-(i)), the model’s output aligns closely with the ordinal structure, demonstrating strong unimodality and low uncertainty. For both $k < y_n$ and $k \geq y_n$, $\mathcal{L}_{\text{ORCU}}$ applies a minimal gradient from \mathcal{L}_{REG} , thereby preserving the existing unimodality and enhancing calibration. This additional gradient addresses the limitations of using \mathcal{L}_{SCE} alone, which can restrict target outputs and lead to underconfident predictions.

When considering the region $k \geq y_n$: as $r \approx -1/t^2$, the model encounters a heightened risk of violating unimodality

and increased uncertainty. At this boundary, the log-barrier function within \mathcal{L}_{REG} dynamically amplifies the gradient on z_k to accommodate this elevated uncertainty. For $k = y_n$, the gradient incrementally raises the correct label’s logit, refining predictions under uncertainty. For $k > y_n$, the gradient raises non-target logits; due to the properties of the softmax function, this increase naturally lowers the target label’s confidence, aligning it with the uncertainty level. In cases where $r > -1/t^2$ (see Figure 2-(ii)), the gradient stabilizes at a fixed, intensified correction of $-t$, maintaining the corrective logic but with a more robust effect. This mechanism effectively balances calibration and ensures that the model preserves the ordinal structure, seamlessly adapting to varying levels of uncertainty.

4. Results

4.1. Datasets and Implementation Details

We evaluated the proposed ORCU loss function on four public datasets with distinct ordinal properties and diverse application domains. The **Image Aesthetics** (IA) dataset (Schifanella et al., 2015) comprises images annotated with 5 levels of aesthetic scores. The **Adience** dataset (Eidinger et al., 2014) is employed for age estimation, consisting of images categorized into 8 age groups. The **LIMUC** dataset (Polat et al., 2022b), annotated with the 4-level Mayo Endoscopic Scores (MES), and a uniformly sampled version of the **Diabetic Retinopathy** (DR) dataset¹, labeled into 5 levels of DR severity, represent medical ordinal classification tasks. Further details on the datasets, data splits, and cross-validation protocols are provided in Appendix B.1.

The ORCU implementation utilized a squared distance metric for soft encoding, with the parameter t determined as $t = 3.0$ based on experiments conducted on the validation set of the balanced DR dataset. All experiments employed ResNet-50 (He et al., 2015) pretrained on ImageNet (Deng et al., 2009), with additional evaluations performed using ResNet-34 and ResNet-101 to ensure robustness. Comprehensive implementation details, including experiments related to t , are provided in Appendix B.2.

4.2. Performance Metrics

Evaluating calibration is essential in ordinal classification tasks, where models must provide not only accurate predictions but also reliable confidence estimates. We emphasize the significance of Static Calibration Error (SCE) and Adaptive Calibration Error (ACE) as robust calibration metrics, especially in addressing class imbalances and per-class

¹<https://www.kaggle.com/datasets/benjaminwarner/resized-2015-2019-blindness-detection-images/data>

calibration analysis. Unlike Expected Calibration Error (ECE), which uniformly measures calibration across all predictions, SCE computes class-specific calibration, making it more suitable for multi-class tasks with ordinal labels (Nixon et al., 2019). ACE further refines ECE by dynamically adjusting bin sizes to evenly distribute predictions, thus addressing skew and providing a more precise measure of confidence reliability in imbalanced datasets (Nixon et al., 2019). These characteristics make SCE and ACE particularly well-suited for calibration assessment in our multi-class ordinal classification context.

To evaluate the order-awareness of our proposed loss function, we employ %Unimodality (%Unimodal) metric, which quantifies how frequently the model produces unimodal probability distributions, indicating its alignment with the ordinal structure (Cardoso et al., 2023). For classification performance, we report accuracy, quadratic weighted kappa (QWK) (Ben-David, 2008), and Mean Absolute Error (MAE). QWK is particularly valuable as it penalizes larger classification errors more heavily and captures ordinal relationships between classes, providing a comprehensive assessment of ordinal classification performance while complementing standard accuracy metrics. Detailed explanations of these metrics are provided in Appendix C.

4.3. Results and Analysis

The proposed loss function, ORCU, establishes a new benchmark by effectively integrating calibration with ordinal relationship modeling. It addresses overconfidence and underconfidence in traditional loss functions, providing reliable confidence estimates for ordinal tasks (Figure 4). Furthermore, the combination of calibration and a well-learned ordinal structure produces well-organized feature embeddings (Figure 5) and input-specific softmax distributions (Figure 6). Comprehensive evaluations against ten loss functions, grouped into ordinal-focused (e.g., SORD (Diaz & Marathe, 2019), CDW-CE (Polat et al., 2022a), CO2 (Albuquerque et al., 2021), POE (Li et al., 2021)) and calibration-focused (e.g., LS (Szegedy et al., 2016), FLSD (Mukhoti et al., 2020), MbLS (Liu et al., 2022), MDCA (Hebbalaguppe et al., 2022), ACLS (Park et al., 2023)), as well as the baseline CE, demonstrate its effective integration of calibration and ordinal learning (Table 2 and Figure 3). These makes ORCU highly suitable for critical applications such as medical diagnosis and rating assessments, where predictive reliability and order-awareness are essential.

4.3.1. JOINT CALIBRATION AND ORDINAL OPTIMIZATION

Overall Performance Evaluation: ORCU strikes an effective balance between calibration and ordinal relationship learning, consistently surpassing existing methods that

Table 2. Calibration performance (SCE, ACE, and ECE) and ordinal structure representation (%Unimodal) across various loss functions on four ordinal datasets. The table shows the mean and standard deviation across folds, highlighting the best in bold and the second-best underlined.

Loss	Metric	SCE↓	ACE↓	ECE↓	%Unimodal↑
Image Aesthetics (n = 13,364)					
CE (Baseline)		0.7637 ± 0.0037	0.7558 ± 0.0035	0.2057 ± 0.0162	96.76 ± 1.59
Ordinal-focused	SORD (Diaz & Marathe, 2019)	<u>0.6844 ± 0.0018</u>	<u>0.6833 ± 0.0018</u>	0.1846 ± 0.0026	100.0 ± 0.00
	CDW-CE (Polat et al., 2022a)	0.7519 ± 0.0030	0.7480 ± 0.0026	0.1751 ± 0.0136	<u>99.71 ± 0.43</u>
	CO2 (Albuquerque et al., 2021)	0.7699 ± 0.0032	0.7614 ± 0.0036	0.2269 ± 0.0151	94.00 ± 1.61
	POE (Li et al., 2021)	0.7612 ± 0.0040	0.7547 ± 0.0043	0.2014 ± 0.0093	89.60 ± 1.90
	Calibration-focused	LS (Szegedy et al., 2016)	0.7222 ± 0.0010	0.7179 ± 0.0014	<u>0.0991 ± 0.0062</u>
	FLSD (Mukhoti et al., 2020)	0.7541 ± 0.0045	0.7482 ± 0.0054	0.1837 ± 0.0121	98.07 ± 0.95
	MbLS (Liu et al., 2022)	0.7577 ± 0.0016	0.7510 ± 0.0020	0.1895 ± 0.0062	84.97 ± 1.14
	MDCA (Hebbalaguppe et al., 2022)	0.7620 ± 0.0033	0.7549 ± 0.0033	0.2022 ± 0.0124	96.32 ± 1.27
	ACLS (Park et al., 2023)	0.7595 ± 0.0014	0.7535 ± 0.0013	0.1957 ± 0.0097	84.61 ± 0.76
	ORCU (Ours)	0.6447 ± 0.0022	0.6419 ± 0.0019	0.0257 ± 0.0040	100.0 ± 0.00
Adience (n = 17,423)					
CE (Baseline)		0.8495 ± 0.0033	0.8356 ± 0.0068	0.3364 ± 0.0401	85.16 ± 1.32
Ordinal-focused	SORD (Diaz & Marathe, 2019)	<u>0.7823 ± 0.0105</u>	<u>0.7783 ± 0.0102</u>	0.0731 ± 0.0240	98.76 ± 0.95
	CDW-CE (Polat et al., 2022a)	0.8429 ± 0.0062	0.8372 ± 0.0071	0.2913 ± 0.0210	93.63 ± 0.89
	CO2 (Albuquerque et al., 2021)	0.8521 ± 0.0055	0.8368 ± 0.0080	0.3533 ± 0.0406	82.36 ± 1.73
	POE (Li et al., 2021)	0.8343 ± 0.0028	0.8240 ± 0.0043	0.2669 ± 0.0363	70.21 ± 0.56
	Calibration-focused	LS (Szegedy et al., 2016)	0.8195 ± 0.0071	0.8101 ± 0.0072	0.1890 ± 0.0415
	FLSD (Mukhoti et al., 2020)	0.8474 ± 0.0063	0.8340 ± 0.0062	0.3193 ± 0.0407	86.65 ± 0.95
	MbLS (Liu et al., 2022)	0.8400 ± 0.0043	0.8295 ± 0.0049	0.2815 ± 0.0344	69.38 ± 0.82
	MDCA (Hebbalaguppe et al., 2022)	0.8496 ± 0.0043	0.8365 ± 0.0056	0.3372 ± 0.0411	84.55 ± 2.41
	ACLS (Park et al., 2023)	0.8398 ± 0.0040	0.8295 ± 0.0045	0.2847 ± 0.0378	68.96 ± 0.91
	ORCU (Ours)	0.4193 ± 0.0218	0.4148 ± 0.0212	0.0880 ± 0.0227	99.94 ± 0.04
LIMUC (n = 11,276)					
CE (Baseline)		0.6997 ± 0.0076	0.6948 ± 0.0075	0.1295 ± 0.0170	97.98 ± 1.20
Ordinal-focused	SORD (Diaz & Marathe, 2019)	<u>0.6382 ± 0.0031</u>	<u>0.6370 ± 0.0032</u>	0.1636 ± 0.0064	100.0 ± 0.00
	CDW-CE (Polat et al., 2022a)	0.6980 ± 0.0048	0.6927 ± 0.0042	0.1190 ± 0.0096	<u>99.86 ± 0.32</u>
	CO2 (Albuquerque et al., 2021)	0.7105 ± 0.0044	0.7042 ± 0.0042	0.1544 ± 0.0118	96.93 ± 1.46
	POE (Li et al., 2021)	0.6996 ± 0.0043	0.6946 ± 0.0044	0.1341 ± 0.0139	89.08 ± 1.03
	Calibration-focused	LS (Szegedy et al., 2016)	0.6647 ± 0.0010	0.6603 ± 0.0022	0.0592 ± 0.0088
	FLSD (Mukhoti et al., 2020)	0.6903 ± 0.0080	0.6853 ± 0.0032	0.1069 ± 0.0167	98.61 ± 1.06
	MbLS (Liu et al., 2022)	0.6928 ± 0.0016	0.6933 ± 0.0013	0.1301 ± 0.0090	85.03 ± 1.31
	MDCA (Hebbalaguppe et al., 2022)	0.6931 ± 0.0058	0.6879 ± 0.0061	0.1197 ± 0.0129	98.19 ± 0.99
	ACLS (Park et al., 2023)	0.6995 ± 0.0035	0.6939 ± 0.0032	0.1299 ± 0.0140	84.58 ± 1.34
	ORCU (Ours)	0.5133 ± 0.0056	0.5105 ± 0.0062	0.0654 ± 0.0073	100.0 ± 0.00
Retinopathy (n = 9,570)					
CE (Baseline)		0.7083 ± 0.0057	0.7050 ± 0.0049	0.2348 ± 0.0057	90.34 ± 0.97
Ordinal-focused	SORD (Diaz & Marathe, 2019)	<u>0.6204 ± 0.0026</u>	<u>0.6196 ± 0.0023</u>	<u>0.0427 ± 0.0023</u>	99.00 ± 0.04
	CDW-CE (Polat et al., 2022a)	0.6978 ± 0.0045	0.6933 ± 0.0044	0.2151 ± 0.0165	99.99 ± 0.01
	CO2 (Albuquerque et al., 2021)	0.7271 ± 0.0044	0.7217 ± 0.0045	0.2867 ± 0.0166	87.68 ± 1.39
	POE (Li et al., 2021)	0.6854 ± 0.0130	0.6817 ± 0.0132	0.1772 ± 0.0265	92.03 ± 2.22
	Calibration-focused	LS (Szegedy et al., 2016)	0.6759 ± 0.0031	0.6730 ± 0.0024	0.1439 ± 0.0139
	FLSD (Mukhoti et al., 2020)	0.6872 ± 0.0031	0.6838 ± 0.0041	0.1790 ± 0.0185	93.01 ± 0.82
	MbLS (Liu et al., 2022)	0.7033 ± 0.0052	0.6997 ± 0.0046	0.2138 ± 0.0164	84.26 ± 1.27
	MDCA (Hebbalaguppe et al., 2022)	0.7077 ± 0.0073	0.7039 ± 0.7039	0.2245 ± 0.0214	91.13 ± 1.52
	ACLS (Park et al., 2023)	0.7074 ± 0.0042	0.7036 ± 0.0053	0.2332 ± 0.0119	84.54 ± 1.07
	ORCU (Ours)	0.5471 ± 0.0126	0.5463 ± 0.0131	0.0322 ± 0.0080	99.96 ± 0.02

prioritize only one aspect. As shown in Table 2, ORCU significantly reduces the calibration errors in all datasets while effectively capturing ordinal relationships between labels. Compared to SORD, ORCU not only improves ordinal alignment but achieves substantial enhancements in calibration metrics such as SCE and ACE. While ECE remains a widely used general-purpose calibration metric, its reliance on binning schemes (Roelofs et al., 2022) and its binary nature (Silva Filho et al., 2023) limit its applicability to multi-class and ordinal tasks. In contrast, SCE and ACE address these limitations by providing detailed class-specific calibration assessments and accommodating imbalanced datasets, making them more suitable for ordinal

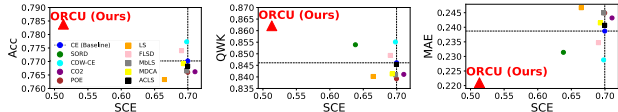


Figure 3. Accuracy, QWK, and MAE vs. SCE on the LIMUC dataset. The plot illustrates the trade-off between prediction and calibration, with models near the top-left (lower SCE, higher Acc/QWK) or bottom-left (lower SCE, lower MAE) indicating optimal performance. ORCU (red triangle) achieves a strong balance between calibration and classification.

tasks. Although LS performs well on ECE, it struggles with SCE and ACE, reflecting its inability to meet the calibration requirements of ordinal tasks. ORCU, on the other hand, demonstrates consistently high performance across all metrics, with particularly robust results on SCE and ACE. This validates the effectiveness of its ordinal-aware regularization in achieving both calibration and a coherent ordinal structure.

Although existing loss functions for ordinal tasks capture label relationships to some extent, they often fail to outperform baseline methods (e.g., CE) and prove insufficient in providing reliable confidence estimates. Similarly, calibration-focused approaches struggle to reduce calibration errors effectively in ordinal tasks and, in some cases, underperform compared to baselines. These challenges emphasize the importance of a unified approach that combines ordinal relationship learning with calibration. ORCU addresses this need through its ordinal-aware regularization, which enforces unimodality and improves confidence alignment, effectively resolving the dual challenges of ordinal classification. Performance evaluations on ResNet-34 and ResNet-101, presented in Appendix D.1, further demonstrate its generalizability.

Figure 3 presents the classification performance metrics of ORCU on the LIMUC dataset. Across all metrics, ORCU consistently achieves optimal performance, demonstrating the lowest SCE, the highest QWK and accuracy, and the lowest MAE. Despite the inherent trade-off between calibration and accuracy during the calibration process (Minderer et al., 2021), ORCU effectively improves network calibration across classes while simultaneously enhancing classification performance. These results demonstrate the comprehensive advantages of ORCU in jointly optimizing calibration and predictive quality for ordinal classification tasks. Comparative analyses, numerical results for other datasets, and Grad-CAM (Gildenblat & contributors, 2021) visualizations illustrating the model’s classification reasoning are provided in Appendix D.2 and Appendix D.3.4.

Calibration Reliability Analysis: Figure 4 provides a visual representation of the calibration performance of the proposed loss function in comparison with CE, SORD, and

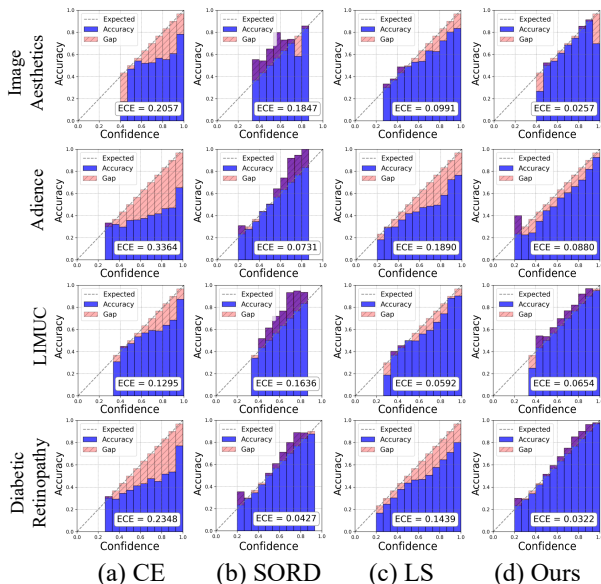


Figure 4. Reliability diagrams for various ordinal loss functions. It illustrates model confidence and the calibration gap between confidence and accuracy on the test split of IA, Adience, LIMUC, and DR. Accuracy bars extending above the expected line indicate underconfidence ($P(Y = y | \hat{P} = p) > p$). In contrast, those below it indicate overconfidence ($P(Y = y | \hat{P} = p) < p$). ECE is computed using 15 bins.

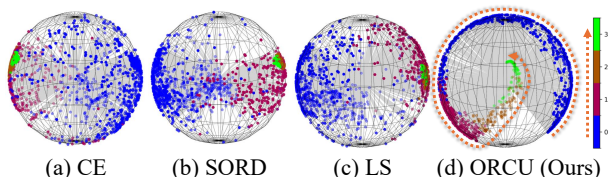


Figure 5. t-SNE visualization of feature embeddings from ResNet-50 trained with CE, SORD, LS, and ORCU on the LIMUC dataset. Colors indicate class labels, and the orange dashed line represents feature alignment, illustrating effective ordinal learning.

LS, using reliability diagrams². CE and LS (Figure 4-(a) and (c)) exhibit overconfidence, as their predictions frequently fall below the expected calibration line. In contrast, SORD (Figure 4-(b)) employs a soft-encoded process to capture ordinal relationships; however, this leads to underconfident predictions and a restricted confidence range. The proposed ORCU (Figure 4-(d)) effectively mitigates SORD’s limitations by incorporating an ordinal-aware regularization term, resulting in more reliable confidence estimates. These results demonstrate the effectiveness of the ordinal-aware calibration mechanism in \mathcal{L}_{ORCU} . Comprehensive results are available in Appendix Appendix D.3.1.

Ordinal Structure and Consistency Assessment: The t-

²https://github.com/Jonathan-Pearce/calibration_library

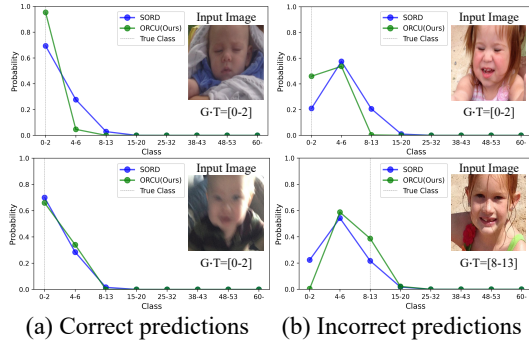


Figure 6. Output distributions of models trained with SORD and ORCU on the test split of the Adience dataset for (a) correct and (b) incorrect predictions. ORCU (green) and SORD (blue) are compared in each subfigure, with the gray dashed line indicating the ground-truth age group.

SNE visualizations³ in Figure 5 illustrate how different loss functions capture ordinal relationships within the embedding space on the LIMUC dataset. This analysis includes the baseline CE, a commonly used loss that lacks ordinal awareness; SORD, designed to model ordinal relationships; LS, a calibration-focused loss selected for its competitive ECE performance (Table 2); and the proposed ORCU, which integrates both calibration and ordinal structure learning. CE and LS (Figure 5-(a), (c)) produce dispersed features without an organized ordinal structure, reflecting their inability to capture ordinal relationships. SORD (Figure 5-(b)), despite its ordinal focus, fails to produce embeddings that fully align with the ordinal label sequence. In contrast, ORCU (Figure 5-(d)) generates a well-structured feature distribution with features organized according to label order, demonstrating the effectiveness of its ordinal-aware regularization term. Additional results are available in Appendix D.3.2.

To further analyze model behavior in ordinal tasks, Figure 6 examines the softmax output distributions of ORCU and SORD on the Adience dataset for both correct and incorrect predictions. For correct predictions (Figure 6-(a)), SORD generates uniform confidence levels, disregarding input-specific uncertainty and failing to adapt dynamically. For incorrect predictions (Figure 6-(b)), SORD produces symmetric distributions, assigning similar probabilities to labels near the predicted label, irrespective of their relation to the ground truth. These limitations arise from SORD’s reliance on distance-based encoding, restricting its ability to capture input-specific variations. In contrast, ORCU adjusts confidence levels dynamically based on input characteristics, refining confidence for the correct label according to input uncertainty. Furthermore, it assigns higher probabilities to labels closer to the true label, achieving both accurate predictions and a consistent ordinal structure. Comparisons

³<https://github.com/needyllove/OrdinalEntropy>

Table 3. Ablation studies on the choice of \mathcal{L}_{REG} and distance metrics used in \mathcal{L}_{SCE} on the DR dataset. \mathcal{L}_{ORCU} is compared with competing regularization methods (\mathcal{L}_{MBLS} , \mathcal{L}_{MDCA} , and \mathcal{L}_{ACLS}). Effects of using different distance metrics for \mathcal{L}_{SCE} are shown. The first row shows the baseline with only \mathcal{L}_{SCE} (Squared) as in SORD.

Combination		Metric	SCE↓	ACE↓	ECE↓	%Unimodal↑
$\mathcal{L}_{SCE}(\phi=\{\})$ + $\mathcal{L}_{\{\}}_{REG}$			Diabetic Retinopathy (n=9,570)			
Squared	+		0.6204 ± 0.0026	0.6196 ± 0.0023	0.0427 ± 0.0023	99.90 ± 0.04
"	+	MbLS	0.6208 ± 0.0031	0.6200 ± 0.0036	0.0465 ± 0.0066	99.27 ± 0.18
"	+	MDCA	0.6221 ± 0.0021	0.6210 ± 0.0008	0.0471 ± 0.0108	99.93 ± 0.02
"	+	ACLS	0.6199 ± 0.0031	0.6198 ± 0.0035	0.0507 ± 0.0110	99.43 ± 0.17
"	+	ORCU(Ours)	0.5471 ± 0.0126	0.5463 ± 0.0131	0.0322 ± 0.0080	99.96 ± 0.02
Absolute	+	"	0.6266 ± 0.0061	0.6253 ± 0.0064	0.0400 ± 0.0038	99.98 ± 0.02
Huber	+	"	0.6222 ± 0.0042	0.6217 ± 0.0047	0.0457 ± 0.0128	99.98 ± 0.01
Exponential	+	"	0.6201 ± 0.0022	0.6187 ± 0.0018	0.0668 ± 0.0174	99.98 ± 0.01

with other loss functions are presented in Appendix D.3.3.

4.3.2. ABLATION STUDY

To analyze the impact of the proposed loss’s regularization term and the choice of distance metric in soft encoding, Table 3 presents the ablation study results conducted on the DR dataset. This analysis demonstrates the importance of an ordinal-aware regularization term for effective ordinal tasks. Conventional calibration regularization terms that ignore inter-class ordinal relationships disrupt the ordinal structure learned by \mathcal{L}_{SCE} and fail to improve calibration. These shows the necessity of ordinal-aware conditioning to calibrate ordinal tasks effectively. Among the evaluated distance metrics, the Squared metric consistently outperformed others, confirming its suitability for this application. These findings validate the effectiveness of ORCU, which integrates Squared-based soft encoding with a regularization term to jointly achieve ordinal structure learning and calibration. Additional results are provided in Appendix D.4.

5. Limitation and Future Work

Although we primarily experimented with computer vision datasets, ORCU has the potential to be employed in various domains such as text, audio, and video. The future study will optimize the parameters for different domains and validate the method. Moreover, we plan to address the remaining miscalibration at extreme confidence levels, which are observed in the reliability diagrams.

6. Conclusion

We proposed ORCU, a novel loss function that improves calibration and unimodality within a unified framework for ordinal classification. By combining soft encoding with an ordinal-aware regularization term, ORCU preserves ordinal relationships while providing reliable confidence estimates. Extensive experiments demonstrate its effectiveness in jointly optimizing calibration and predictive accuracy, addressing critical limitations of existing approaches. ORCU

establishes a robust foundation for advancing reliable ordinal classification and paves the way for future research into methodologies that seamlessly integrate calibration and ordinal structure across various applications.

References

- Albuquerque, T., Cruz, R., and Cardoso, J. S. Ordinal losses for classification of cervical cancer risk. *PeerJ Computer Science*, 7:e457, 2021.
- Belharbi, S., Ayed, I. B., McCaffrey, L., and Granger, E. Non-parametric uni-modality constraints for deep ordinal classification. *arXiv preprint arXiv:1911.10720*, 2019.
- Ben-David, A. Comparison of classification accuracy using cohen’s weighted kappa. *Expert Systems with Applications*, 34(2):825–832, 2008.
- Buslaev, A., Iglovikov, V. I., Khvedchenya, E., Parinov, A., Druzhinin, M., and Kalinin, A. A. Albuementations: Fast and flexible image augmentations. *Information*, 11(2):125, February 2020. ISSN 2078-2489. doi: 10.3390/info11020125. URL <http://dx.doi.org/10.3390/info11020125>.
- Cao, W., Mirjalili, V., and Raschka, S. Rank consistent ordinal regression for neural networks with application to age estimation. *Pattern Recognition Letters*, 140:325–331, 2020.
- Cardoso, J. S., Cruz, R., and Albuquerque, T. Unimodal distributions for ordinal regression. *arXiv preprint arXiv:2303.04547*, 2023.
- Chen, S., Zhang, C., Dong, M., Le, J., and Rao, M. Using ranking-cnn for age estimation. In *Proceedings of the IEEE conference on computer vision and pattern recognition*, pp. 5183–5192, 2017.
- Deng, J., Dong, W., Socher, R., Li, L.-J., Li, K., and Fei-Fei, L. Imagenet: A large-scale hierarchical image database. In *2009 IEEE conference on computer vision and pattern recognition*, pp. 248–255. Ieee, 2009.
- Dey, P., Merugu, S., and Kaveri, S. R. Conformal prediction sets for ordinal classification. *Advances in Neural Information Processing Systems*, 36, 2024.
- Diaz, R. and Marathe, A. Soft labels for ordinal regression. In *Proceedings of the IEEE/CVF conference on computer vision and pattern recognition*, pp. 4738–4747, 2019.
- Eidinger, E., Enbar, R., and Hassner, T. Age and gender estimation of unfiltered faces. *IEEE Transactions on information forensics and security*, 9(12):2170–2179, 2014.
- Fu, Y. and Huang, T. S. Human age estimation with regression on discriminative aging manifold. *IEEE Transactions on Multimedia*, 10(4):578–584, 2008.
- Gildenblat, J. and contributors. Pytorch library for cam methods. <https://github.com/jacobgil/pytorch-grad-cam>, 2021.
- Guo, C., Pleiss, G., Sun, Y., and Weinberger, K. Q. On calibration of modern neural networks. In *International conference on machine learning*, pp. 1321–1330. PMLR, 2017.
- He, K., Zhang, X., Ren, S., and Sun, J. Deep residual learning for image recognition, 2015. URL <https://arxiv.org/abs/1512.03385>.
- Hebbalaguppe, R., Prakash, J., Madan, N., and Arora, C. A stitch in time saves nine: A train-time regularizing loss for improved neural network calibration. In *Proceedings of the IEEE/CVF Conference on Computer Vision and Pattern Recognition*, pp. 16081–16090, 2022.
- Jiang, X., Osl, M., Kim, J., and Ohno-Machado, L. Calibrating predictive model estimates to support personalized medicine. *Journal of the American Medical Informatics Association*, 19(2):263–274, 2012.
- Kompa, B., Snoek, J., and Beam, A. L. Second opinion needed: communicating uncertainty in medical machine learning. *NPJ Digital Medicine*, 4(1):4, 2021.
- Li, Q., Wang, J., Yao, Z., Li, Y., Yang, P., Yan, J., Wang, C., and Pu, S. Unimodal-concentrated loss: Fully adaptive label distribution learning for ordinal regression. In *Proceedings of the IEEE/CVF Conference on Computer Vision and Pattern Recognition*, pp. 20513–20522, 2022.
- Li, W., Lu, J., Feng, J., Xu, C., Zhou, J., and Tian, Q. Bridgenet: A continuity-aware probabilistic network for age estimation. In *Proceedings of the IEEE/CVF conference on computer vision and pattern recognition*, pp. 1145–1154, 2019.
- Li, W., Huang, X., Lu, J., Feng, J., and Zhou, J. Learning probabilistic ordinal embeddings for uncertainty-aware regression. In *Proceedings of the IEEE/CVF conference on computer vision and pattern recognition*, pp. 13896–13905, 2021.
- Liu, B., Ben Ayed, I., Galdran, A., and Dolz, J. The devil is in the margin: Margin-based label smoothing for network calibration. In *Proceedings of the IEEE/CVF Conference on Computer Vision and Pattern Recognition*, pp. 80–88, 2022.
- Liu, X., Fan, F., Kong, L., Diao, Z., Xie, W., Lu, J., and You, J. Unimodal regularized neuron stick-breaking for ordinal classification. *Neurocomputing*, 388:34–44, 2020.

- Loshchilov, I. and Hutter, F. Decoupled weight decay regularization, 2019. URL <https://arxiv.org/abs/1711.05101>.
- Minderer, M., Djolonga, J., Romijnders, R., Hubis, F., Zhai, X., Houlsby, N., Tran, D., and Lucic, M. Revisiting the calibration of modern neural networks. *Advances in Neural Information Processing Systems*, 34:15682–15694, 2021.
- Moon, J., Kim, J., Shin, Y., and Hwang, S. Confidence-aware learning for deep neural networks. In *international conference on machine learning*, pp. 7034–7044. PMLR, 2020.
- Mukhoti, J., Kulharia, V., Sanyal, A., Golodetz, S., Torr, P., and Dokania, P. Calibrating deep neural networks using focal loss. *Advances in Neural Information Processing Systems*, 33:15288–15299, 2020.
- Neumann, L., Zisserman, A., and Vedaldi, A. Relaxed softmax: Efficient confidence auto-calibration for safe pedestrian detection. 2018.
- Niu, Z., Zhou, M., Wang, L., Gao, X., and Hua, G. Ordinal regression with multiple output cnn for age estimation. In *Proceedings of the IEEE Conference on Computer Vision and Pattern Recognition (CVPR)*, June 2016.
- Nixon, J., Dusenberry, M. W., Zhang, L., Jerfel, G., and Tran, D. Measuring calibration in deep learning. In *CVPR workshops*, volume 2, 2019.
- Pan, H., Han, H., Shan, S., and Chen, X. Mean-variance loss for deep age estimation from a face. In *Proceedings of the IEEE conference on computer vision and pattern recognition*, pp. 5285–5294, 2018.
- Paplhám, J., Franc, V., et al. A call to reflect on evaluation practices for age estimation: Comparative analysis of the state-of-the-art and a unified benchmark. In *Proceedings of the IEEE/CVF Conference on Computer Vision and Pattern Recognition*, pp. 1196–1205, 2024.
- Park, H., Noh, J., Oh, Y., Baek, D., and Ham, B. Acls: Adaptive and conditional label smoothing for network calibration. In *Proceedings of the IEEE/CVF International Conference on Computer Vision*, pp. 3936–3945, 2023.
- Platt, J. et al. Probabilistic outputs for support vector machines and comparisons to regularized likelihood methods. *Advances in large margin classifiers*, 10(3):61–74, 1999.
- Polat, G., Ergenc, I., Kani, H. T., Alahdab, Y. O., Atug, O., and Temizel, A. Class distance weighted cross-entropy loss for ulcerative colitis severity estimation. In *Annual Conference on Medical Image Understanding and Analysis*, pp. 157–171. Springer, 2022a.
- Polat, G., Kani, H., Ergenc, I., Alahdab, Y., Temizel, A., and Atug, O. Labeled images for ulcerative colitis (limuc) dataset. *Accessed March*, 2022b.
- Roelofs, R., Cain, N., Shlens, J., and Mozer, M. C. Mitigating bias in calibration error estimation. In *International Conference on Artificial Intelligence and Statistics*, pp. 4036–4054. PMLR, 2022.
- Russakovsky, O., Deng, J., Su, H., Krause, J., Satheesh, S., Ma, S., Huang, Z., Karpathy, A., Khosla, A., Bernstein, M., et al. Imagenet large scale visual recognition challenge. *International journal of computer vision*, 115: 211–252, 2015.
- Schifanella, R., Redi, M., and Aiello, L. M. An image is worth more than a thousand favorites: Surfacing the hidden beauty of flickr pictures. In *Proceedings of the international AAAI conference on web and social media*, volume 9, pp. 397–406, 2015.
- Shi, X., Cao, W., and Raschka, S. Deep neural networks for rank-consistent ordinal regression based on conditional probabilities. *Pattern Analysis and Applications*, 26(3): 941–955, 2023.
- Silva Filho, T., Song, H., Perello-Nieto, M., Santos-Rodriguez, R., Kull, M., and Flach, P. Classifier calibration: a survey on how to assess and improve predicted class probabilities. *Machine Learning*, 112(9): 3211–3260, 2023.
- Song, H., Diethe, T., Kull, M., and Flach, P. Distribution calibration for regression. In *International Conference on Machine Learning*, pp. 5897–5906. PMLR, 2019.
- Suara, S., Jha, A., Sinha, P., and Sekh, A. A. Is gradcam explainable in medical images? In *International Conference on Computer Vision and Image Processing*, pp. 124–135. Springer, 2023.
- Szegedy, C., Vanhoucke, V., Ioffe, S., Shlens, J., and Wojna, Z. Rethinking the inception architecture for computer vision. In *Proceedings of the IEEE conference on computer vision and pattern recognition*, pp. 2818–2826, 2016.
- Tan, Z., Yang, X., Wang, Q., Nguyen, A., and Huang, K. Interpret your decision: Logical reasoning regularization for generalization in visual classification. *arXiv preprint arXiv:2410.04492*, 2024.
- Tomani, C., Gruber, S., Erdem, M. E., Cremers, D., and Buettner, F. Post-hoc uncertainty calibration for domain drift scenarios. In *Proceedings of the IEEE/CVF Conference on Computer Vision and Pattern Recognition*, pp. 10124–10132, 2021.

- Tomani, C., Cremers, D., and Buettner, F. Parameterized temperature scaling for boosting the expressive power in post-hoc uncertainty calibration. In *European Conference on Computer Vision*, pp. 555–569. Springer, 2022.
- Vaicenavicius, J., Widmann, D., Andersson, C., Lindsten, F., Roll, J., and Schön, T. Evaluating model calibration in classification. In *The 22nd international conference on artificial intelligence and statistics*, pp. 3459–3467. PMLR, 2019.
- Vargas, V. M., Gutiérrez, P. A., and Hervás-Martínez, C. Unimodal regularisation based on beta distribution for deep ordinal regression. *Pattern Recognition*, 122: 108310, 2022.
- Yang, T.-Y., Huang, Y.-H., Lin, Y.-Y., Hsiu, P.-C., and Chuang, Y.-Y. Ssr-net: A compact soft stagewise regression network for age estimation. In *IJCAI*, volume 5, pp. 7, 2018.

A. Summary

This supplementary material provides additional details and analyses to complement the findings presented in the main paper. Specifically:

- Appendix B summarizes the datasets and implementation details.
- Appendix C details the performance metrics used to evaluate calibration and classification performance.
- Appendix D presents extended results on classification and generalization performance (Appendix D.1 and Appendix D.2) as well as visual analyses (Appendix D.3) such as reliability diagrams, t-SNE visualizations, softmax output distributions, and Grad-CAM visualizations.
- Appendix D.4 provides an ablation study assessing the contributions of key components in $\mathcal{L}_{\text{ORCU}}$.

These supplementary sections are intended to provide a comprehensive understanding of the methods, results, and analyses supporting the proposed approach.

Table 1. Label-wise distribution of images across all datasets, presented as counts and proportions (%). This table enables the observation of datasets with balanced and imbalanced label distributions.

Datasets Label	Image Aesthetics (Schifanella et al., 2015)	Adience (Eidinger et al., 2014)	LIMUC (Polat et al., 2022b)	Diabetic Retinopathy
0	36 (0.27%)	2,518 (14.45%)	6,105 (54.14%)	1,914 (20.00%)
1	654 (4.89%)	2,163 (12.41%)	3,052 (27.07%)	1,914 (20.00%)
2	8,157 (61.04%)	2,132 (12.24%)	1,254 (11.12%)	1,914 (20.00%)
3	4,211 (31.51%)	1,655 (9.50%)	865 (7.67%)	1,914 (20.00%)
4	306 (2.29%)	4,950 (28.41%)	-	1,914 (20.00%)
5	-	2,300 (13.20%)	-	-
6	-	830 (4.76%)	-	-
7	-	875 (5.02%)	-	-
Total	13,364	17,423	11,276	9,570

B. Datasets and Implementation Details

B.1. Datasets

We evaluated the proposed $\mathcal{L}_{\text{ORCU}}$ loss function on four publicly available datasets, each selected for its ordinal characteristics and relevance to distinct application domains:

- **Image Aesthetics dataset** (Schifanella et al., 2015): This dataset, derived from Flickr, includes 13,364 valid images annotated with 5 ordinal aesthetic score levels, reflecting subjective aesthetic judgments. For evaluation, we employed an 80/20 train-test split and performed five-fold cross-validation to ensure reliable performance measurement.
- **Adience dataset** (Eidinger et al., 2014): The Adience dataset comprises 26,580 images grouped into 8 ordinal age categories and is widely used for age estimation tasks where the inherent order of age groups is critical. Of these, 17,423 images are included in the predefined folds⁴. We evaluated using five-fold cross-validation, leveraging the predefined folds to maintain a consistent train-test split ratio of approximately 80/20.
- **LIMUC dataset** (Polat et al., 2022b): This medical dataset contains 11,276 images of ulcerative colitis patients labeled with 4 ordinal Mayo Endoscopic Scores (MES), representing disease severity. To ensure robust and clinically relevant evaluations, we adopted a subject-exclusive train-test split protocol (Paplhám et al., 2024) with an 85/15 ratio, alongside a ten-fold cross-validation approach (Polat et al., 2022a).

⁴<https://talhassner.github.io/home/projects/Adience/Adience-data.html>

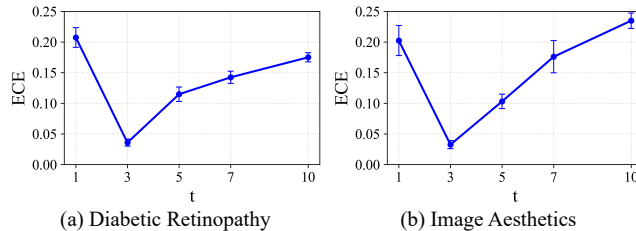


Figure 1. Effect of the parameter t in \mathcal{L}_{ORCU} on ECE. (a) Validation result on the balanced Diabetic Retinopathy dataset was used to determine t . (b) Validation on the imbalanced Image Aesthetics dataset, demonstrating the generalizability of t .

- **Diabetic Retinopathy dataset**⁵: This dataset comprises retinal fundus images from the Kaggle 2015 Diabetic Retinopathy Detection⁶ and APTOS 2019 Blindness Detection⁷ competitions. Each image is resized and cropped to a maximum dimension of 1024×1024 pixels. The images are labeled from 0 to 4 based on the severity of diabetic retinopathy. To address the class imbalance in the original dataset of 88,702 images, we performed uniform sampling based on the class with the smallest sample size (severity level 4), ensuring each class contained 1,914 images. This process resulted in a balanced subset of 9,570 images. For evaluation, we applied an 80/20 train-test split and conducted five-fold cross-validation.

Details on the label distributions for each dataset are provided in Table 1.

B.2. Implementation Details

For most experiments, we employed a ResNet-50 architecture (He et al., 2015) pretrained on ImageNet (Russakovsky et al., 2015) as the backbone. To evaluate the generalizability of the proposed method, we also conducted experiments using ResNet-34 and ResNet-101. All architectures followed the same implementation settings, as detailed below:

- **Learning Strategy:** A layer-wise learning rate was employed, assigning an initial learning rate of 0.01 to the fully connected layer and 0.001 to all other layers. The models were optimized using the AdamW optimizer (Loshchilov & Hutter, 2019) with a weight decay of 0.01. Additionally, we employed a ReduceLROnPlateau scheduler to adapt the learning rate dynamically based on validation loss, ensuring stable convergence.
- **Training Protocol:** Models were trained for 100 epochs with a batch size of 64. Input images were resized to 224×224 pixels before applying augmentation. All training and evaluation procedures were conducted on NVIDIA RTX 4090 GPUs.
- **Data Augmentation:** Data augmentation included vertical and horizontal flipping (each with a probability of 0.5), rotation (up to 20 degrees with a probability of 0.5), and normalization using the mean and standard deviation computed from each dataset’s training set. These augmentations were implemented using the Albumentations library (Buslaev et al., 2020).
- **ORCU:** The \mathcal{L}_{ORCU} loss employed a squared distance metric for soft encoding. To determine the optimal value of the parameter t , experiments were conducted on the validation set of the most balanced dataset, Retinopathy, using $t \in \{1.0, 3.0, 5.0, 7.0, 10.0\}$. The parameter $t = 3.0$, which achieved the lowest ECE (Figure 1-(a)), was selected and subsequently used in all experiments. This selection was further validated on the validation set of the most imbalanced dataset, Image Aesthetics, where the parameter $t = 3.0$ also achieved the lowest ECE (Figure 1-(b)), demonstrating its effectiveness and generalizability across datasets.

C. Performance Metrics

This section provides detailed descriptions of the metrics used to evaluate calibration and classification performance in our experiments. While Expected Calibration Error (ECE) has been extensively utilized to assess calibration, its applicability to

⁵<https://www.kaggle.com/datasets/benjaminwarner/resized-2015-2019-blindness-detection-images/data>

⁶<https://www.kaggle.com/c/diabetic-retinopathy-detection>

⁷<https://www.kaggle.com/c/aptos2019-blindness-detection>

multi-class and ordinal tasks is limited. To address these limitations, we incorporate Static Calibration Error (SCE) and Adaptive Calibration Error (ACE), which are specifically designed to offer more effective calibration evaluation in such contexts (Nixon et al., 2019). For classification performance, we present traditional metrics such as Accuracy (Acc) and Mean Absolute Error (MAE), along with Quadratic Weighted Kappa (QWK) (Ben-David, 2008), which reflects ordinal relationships, and %Unimodality (Cardoso et al., 2023), which evaluates the model’s alignment with ordinal structures.

C.1. Calibration Metrics

To evaluate how well model predictions align with their confidence estimates, we employ several calibration metrics. Among these, Expected Calibration Error (ECE) is one of the most widely used metrics due to its simplicity and effectiveness in general classification settings. ECE discretizes the $[0, 1]$ probability interval into B equally spaced bins. For each bin b , the accuracy $\text{acc}(b)$ is the fraction of correctly predicted samples, and the confidence $\text{conf}(b)$ is the average predicted probability of the samples in that bin. ECE is defined as:

$$\text{ECE} = \sum_{b=1}^B \frac{n_b}{N} |\text{acc}(b) - \text{conf}(b)|, \tag{1}$$

where n_b is the number of predictions in bin b , and N is the total number of predictions. Despite its widespread use, ECE exhibits limitations in multi-class settings, as it does not account for class-specific calibration and relies on fixed binning, which can lead to biased estimates, particularly in imbalanced datasets.

To address these limitations, Static Calibration Error (SCE) extends ECE by computing calibration errors for each class and averaging them, enabling a finer-grained evaluation of calibration. This makes SCE particularly suitable for tasks involving ordinal labels, where evaluating the overall label structure is crucial. SCE is defined as:

$$\text{SCE} = \frac{1}{K} \sum_{k=1}^K \sum_{b=1}^B \frac{n_{b,k}}{N} |\text{acc}(b, k) - \text{conf}(b, k)|, \tag{2}$$

where $n_{b,k}$ represents the number of predictions in bin b for class k , and $\text{acc}(b, k)$ and $\text{conf}(b, k)$ denote the accuracy and confidence for bin b of class k . By incorporating class-specific calibration, SCE provides greater granularity, essential for multi-class tasks, especially those involving inherent ordinal relationships among labels.

Adaptive Calibration Error (ACE) further enhances SCE by introducing adaptive binning, which ensures an equal number of predictions per bin. This dynamic adjustment mitigates sparsity issues commonly encountered in fixed-bin approaches and enables reliable evaluation in regions with imbalanced class distributions. ACE is defined as:

$$\text{ACE} = \frac{1}{KR} \sum_{k=1}^K \sum_{r=1}^R |\text{acc}(r, k) - \text{conf}(r, k)|, \tag{3}$$

where R is the number of adaptive bins, and $\text{acc}(r, k)$ and $\text{conf}(r, k)$ represent the accuracy and confidence in range r for class k . By dynamically adjusting bin sizes, ACE offers a more precise and reliable calibration measure, making it particularly effective for evaluating models on datasets with highly imbalanced class distributions.

These metrics collectively demonstrate the limitations of ECE in addressing the challenges of multi-class and ordinal settings while illustrating the strengths of SCE and ACE. SCE focuses on class-specific calibration, providing greater detail and precision, whereas ACE improves robustness through adaptive binning, making both metrics essential for evaluating calibration in ordinal classification tasks. Consequently, employing ECE, SCE, and ACE together enables a comprehensive and detailed assessment of calibration performance in such tasks.

C.2. Ordinal Classification Metrics

In this section, we describe the metrics Quadratic Weighted Kappa (QWK) and %Unimodality, which are used to evaluate the classification performance of ORCU based on its ability to capture ordinal relationships.

QWK measures the agreement between predicted and true labels while explicitly accounting for the structured relationships among classes (Ben-David, 2008). Unlike standard accuracy metrics, QWK incorporates a quadratic weighting scheme that

penalizes larger discrepancies more heavily, making it particularly effective for tasks where the relative distance between classes is critical. The metric is defined as:

$$\text{QWK} = 1 - \frac{\sum_{i=1}^C \sum_{j=1}^C w_{ij} O_{ij}}{\sum_{i=1}^C \sum_{j=1}^C w_{ij} E_{ij}}, \quad (4)$$

where C is the number of classes, $w_{ij} = \frac{(i-j)^2}{(C-1)^2}$ is the weight assigned to the disagreement between classes i and j , O_{ij} is the observed count, and E_{ij} is the expected count under random chance. QWK ranges from -1 (complete disagreement) to 1 (perfect agreement), with higher values indicating stronger alignment between predictions and ground truth. By reflecting the severity of misclassifications, QWK complements accuracy as a robust metric for evaluating ordinal classification tasks.

The %Unimodality metric quantifies the proportion of predictions that satisfy the unimodality property with respect to the true label. Let $\hat{y} \in \mathbb{R}^C$ represent the predicted probability distribution over C ordinal labels, and let $y \in \{1, \dots, C\}$ denote the true label. A distribution satisfies the unimodality property if the probabilities increase monotonically up to the true label y and decrease monotonically thereafter. This condition is formally expressed as:

$$\hat{y}_1 \leq \hat{y}_2 \leq \dots \leq \hat{y}_y \quad \text{and} \quad \hat{y}_y \geq \hat{y}_{y+1} \geq \dots \geq \hat{y}_C. \quad (5)$$

For each prediction, let $U \in \{0, 1\}$ indicate unimodality:

$$U = \begin{cases} 1, & \text{if unimodality is satisfied,} \\ 0, & \text{otherwise.} \end{cases} \quad (6)$$

The %Unimodality metric is computed as:

$$\% \text{Unimodality} = \frac{1}{N} \sum_{n=1}^N U_n, \quad (7)$$

where U_n indicates whether unimodality is satisfied for the n -th prediction, and N is the total number of predictions. This metric directly evaluates the model’s ability to produce probability distributions that respect the ordinal relationships among labels.

These two metrics are particularly well-suited for evaluating the performance of the proposed loss, as they effectively measure ORCU’s ability to capture ordinal relationships during learning and produce predictions that align with the structured relationships among labels.

D. Additional Results

D.1. Generalization Performance

This section presents extended results evaluating the generalizability of the proposed $\mathcal{L}_{\text{ORCU}}$ loss function across different model architectures. Table 2 examines calibration performance and the ability to capture ordinal label relationships on the Image Aesthetics, Adience, LIMUC, and Diabetic Retinopathy datasets using ResNet-34 (He et al., 2015) and ResNet-101 architectures. Across both architectures, $\mathcal{L}_{\text{ORCU}}$ consistently achieves low calibration errors while preserving alignment with ordinal label structures, demonstrating its robustness in producing well-calibrated and ordinal-aware predictions. These findings affirm the effectiveness of $\mathcal{L}_{\text{ORCU}}$ for ordinal classification tasks across diverse architectures.

D.2. Classification Performance

Table 3 provides detailed numerical comparisons between $\mathcal{L}_{\text{ORCU}}$ and baseline loss functions, demonstrating its ability to improve calibration with minimal impact on classification performance. $\mathcal{L}_{\text{ORCU}}$ achieves superior prediction performance across all metrics compared to the baseline CE. Furthermore, it delivers competitive results on performance metrics relative to other ordinal loss functions while significantly outperforming calibration-focused losses, owing to its effective utilization of ordinal structures. These results collectively confirm $\mathcal{L}_{\text{ORCU}}$ ’s capacity to optimize the trade-off between calibration and predictive performance by leveraging ordinal relationships.

Calibration of Ordinal Regression Networks

Table 2. Calibration and ordinal consistency performance of various loss functions evaluated on four datasets, including Adience, Image Aesthetics, LIMUC, and Diabetic Retinopathy, using ResNet-34 and ResNet-101 architectures. Metrics include Static Calibration Error (SCE), Adaptive Calibration Error (ACE), Expected Calibration Error (ECE), and %Unimodality (%Unimodal). Results are reported as the mean and standard deviation across folds. The best performance is highlighted in bold, and the second-best is underlined.

Loss	Model	Metrics	ResNet-34				ResNet-101			
			SCE↓	ACE↓	ECE↓	%Unimodal↑	SCE↓	ACE↓	ECE↓	%Unimodal↑
Image Aesthetics ($n=13,364$)										
	CE (Baseline)		0.7533 ± 0.0047	0.7459 ± 0.0048	0.1965 ± 0.0154	99.55 ± 0.54	0.7630 ± 0.0064	0.7557 ± 0.0068	0.2049 ± 0.0220	95.63 ± 1.38
Calibration-focused Ordinal-focused	SORD (Diaz & Marathe, 2019)		<u>0.6805 ± 0.0021</u>	<u>0.6790 ± 0.0042</u>	<u>0.1846 ± 0.0089</u>	100.0 ± 0.00	<u>0.6846 ± 0.0032</u>	<u>0.6835 ± 0.0031</u>	0.1813 ± 0.0101	100.0 ± 0.00
	CDW-CE (Polat et al., 2022a)		0.7017 ± 0.0104	0.7013 ± 0.0101	<u>0.0860 ± 0.0059</u>	93.02 ± 8.91	0.7504 ± 0.0053	0.7471 ± 0.0048	0.1642 ± 0.0161	<u>98.47 ± 1.45</u>
	CO2 (Albuquerque et al., 2021)		0.7623 ± 0.0047	0.7560 ± 0.0033	0.2089 ± 0.0214	99.44 ± 0.49	0.7702 ± 0.0021	0.7622 ± 0.0022	0.2258 ± 0.0081	94.29 ± 0.73
	POE (Li et al., 2021)		0.7314 ± 0.0134	0.7262 ± 0.0122	0.1393 ± 0.0431	95.81 ± 3.15	0.7535 ± 0.0081	0.7469 ± 0.0073	0.1920 ± 0.0112	91.23 ± 1.59
	LS (Szegedy et al., 2016)		0.7182 ± 0.0039	0.7130 ± 0.0043	0.1010 ± 0.0165	82.82 ± 1.68	0.7260 ± 0.0008	0.7221 ± 0.0009	<u>0.1135 ± 0.0057</u>	78.68 ± 0.18
	FLSD (Mukhoti et al., 2020)		0.7351 ± 0.0089	0.7287 ± 0.0084	0.1395 ± 0.0210	99.80 ± 0.24	0.7540 ± 0.0060	0.7466 ± 0.0056	0.1776 ± 0.0216	97.64 ± 0.47
	MbLS (Liu et al., 2022)		0.7496 ± 0.0042	0.7427 ± 0.0040	0.1800 ± 0.0102	90.30 ± 0.99	0.7566 ± 0.0019	0.7500 ± 0.0025	0.1893 ± 0.0079	85.40 ± 1.06
	MDCA (Hebbalaguppe et al., 2022)		0.7478 ± 0.0030	0.7409 ± 0.0037	0.1809 ± 0.0052	<u>99.89 ± 0.09</u>	0.7618 ± 0.0026	0.7540 ± 0.0056	0.2055 ± 0.0056	96.01 ± 0.86
	ACLS (Park et al., 2023)		0.7457 ± 0.0082	0.7391 ± 0.0077	0.1742 ± 0.0238	90.54 ± 3.50	0.7589 ± 0.0016	0.7521 ± 0.0026	0.1943 ± 0.0086	84.64 ± 0.65
	ORCU (Ours)		0.6391 ± 0.0112	0.6369 ± 0.0116	0.0608 ± 0.0401	100.0 ± 0.00	0.6432 ± 0.0033	0.6403 ± 0.0032	0.0220 ± 0.0031	100.0 ± 0.00
Adience ($n=17,423$)										
	CE (Baseline)		0.8470 ± 0.0077	0.8331 ± 0.0076	0.3365 ± 0.0309	84.27 ± 2.71	0.8497 ± 0.0027	0.8355 ± 0.0055	0.3406 ± 0.0486	84.17 ± 1.51
Calibration-focused Ordinal-focused	SORD (Diaz & Marathe, 2019)		<u>0.7849 ± 0.0091</u>	<u>0.7807 ± 0.0107</u>	<u>0.0704 ± 0.0160</u>	<u>97.85 ± 0.77</u>	<u>0.7843 ± 0.0094</u>	<u>0.7810 ± 0.0097</u>	0.0752 ± 0.0295	<u>98.15 ± 0.82</u>
	CDW-CE (Polat et al., 2022a)		0.8469 ± 0.0047	0.8397 ± 0.0041	0.3092 ± 0.0248	88.43 ± 1.83	0.8435 ± 0.0031	0.8373 ± 0.0034	0.3053 ± 0.0353	91.75 ± 2.04
	CO2 (Albuquerque et al., 2021)		0.8503 ± 0.0047	0.8363 ± 0.0073	0.3563 ± 0.0409	81.86 ± 1.65	0.8525 ± 0.0047	0.8376 ± 0.0070	0.3647 ± 0.0401	83.04 ± 1.34
	POE (Li et al., 2021)		0.8452 ± 0.0038	0.8345 ± 0.0048	0.3123 ± 0.0430	70.42 ± 2.22	0.8381 ± 0.0040	0.8285 ± 0.0058	0.2822 ± 0.0286	70.59 ± 1.03
	LS (Szegedy et al., 2016)		0.8305 ± 0.0057	0.8203 ± 0.0079	0.2437 ± 0.0265	66.65 ± 8.32	0.8219 ± 0.0062	0.8122 ± 0.0052	0.2050 ± 0.0413	67.47 ± 0.76
	FLSD (Mukhoti et al., 2020)		0.8477 ± 0.0056	0.8358 ± 0.0078	0.3216 ± 0.0398	85.03 ± 2.23	0.8488 ± 0.0034	0.8354 ± 0.0428	0.3256 ± 0.0063	85.50 ± 0.98
	MbLS (Liu et al., 2022)		0.8487 ± 0.0032	0.8360 ± 0.0060	0.3220 ± 0.0350	69.77 ± 1.09	0.8430 ± 0.0039	0.8308 ± 0.0060	0.2968 ± 0.0418	69.73 ± 0.93
	MDCA (Hebbalaguppe et al., 2022)		0.8500 ± 0.0071	0.8366 ± 0.0094	0.3434 ± 0.0315	83.14 ± 1.94	0.8509 ± 0.0039	0.8375 ± 0.0059	0.3417 ± 0.0363	83.99 ± 1.84
	ACLS (Park et al., 2023)		0.8489 ± 0.0039	0.8353 ± 0.0066	0.3222 ± 0.0366	68.91 ± 1.35	0.8417 ± 0.0041	0.8315 ± 0.0053	0.2865 ± 0.0345	68.79 ± 0.81
	ORCU (Ours)		0.4091 ± 0.0104	0.4057 ± 0.0099	0.0697 ± 0.0232	99.98 ± 0.01	0.4193 ± 0.0169	0.4151 ± 0.0164	0.0896 ± 0.0232	99.92 ± 0.04
LIMUC ($n=11,276$)										
	CE (Baseline)		0.6725 ± 0.0098	0.6681 ± 0.0095	0.0724 ± 0.0234	99.65 ± 0.26	0.7026 ± 0.0066	0.6960 ± 0.0061	0.1313 ± 0.0122	97.92 ± 0.98
Calibration-focused Ordinal-focused	SORD (Diaz & Marathe, 2019)		<u>0.6389 ± 0.0037</u>	<u>0.6375 ± 0.0039</u>	0.1685 ± 0.0117	100.0 ± 0.00	<u>0.6410 ± 0.0040</u>	<u>0.6397 ± 0.0037</u>	0.1614 ± 0.0078	100.0 ± 0.00
	CDW-CE (Polat et al., 2022a)		0.6580 ± 0.0165	0.6533 ± 0.0154	0.0750 ± 0.0319	99.85 ± 0.37	0.7005 ± 0.0047	0.6950 ± 0.0049	0.1176 ± 0.0094	<u>99.85 ± 0.28</u>
	CO2 (Albuquerque et al., 2021)		0.6965 ± 0.0061	0.6906 ± 0.0056	0.1300 ± 0.0166	99.68 ± 0.32	0.7108 ± 0.0077	0.7051 ± 0.0079	0.1517 ± 0.0075	97.54 ± 1.52
	POE (Li et al., 2021)		0.6870 ± 0.0072	0.6820 ± 0.0067	0.1007 ± 0.0212	95.01 ± 2.19	0.7045 ± 0.0033	0.6988 ± 0.0023	0.1360 ± 0.0104	89.62 ± 1.68
	LS (Szegedy et al., 2016)		0.6691 ± 0.0023	0.6646 ± 0.0023	<u>0.0606 ± 0.0146</u>	81.12 ± 2.07	0.6688 ± 0.0015	0.6688 ± 0.0015	0.0584 ± 0.0082	76.83 ± 0.90
	FLSD (Mukhoti et al., 2020)		0.6614 ± 0.0086	0.6569 ± 0.0085	0.0427 ± 0.0133	<u>99.85 ± 0.10</u>	0.7001 ± 0.0028	0.6947 ± 0.0032	0.1230 ± 0.0080	98.36 ± 1.60
	MbLS (Liu et al., 2022)		0.6958 ± 0.0061	0.6907 ± 0.0064	0.1211 ± 0.0184	86.84 ± 2.00	0.7024 ± 0.0026	0.6970 ± 0.0032	0.1331 ± 0.0106	82.97 ± 0.92
	MDCA (Hebbalaguppe et al., 2022)		0.6716 ± 0.0083	0.6693 ± 0.0076	0.0667 ± 0.0192	99.80 ± 0.12	0.6986 ± 0.0054	0.6928 ± 0.0045	0.1272 ± 0.0138	98.40 ± 1.28
	ACLS (Park et al., 2023)		0.6950 ± 0.0053	0.6899 ± 0.0051	0.1209 ± 0.0178	87.57 ± 2.26	0.7040 ± 0.0040	0.6978 ± 0.0037	0.1351 ± 0.0119	82.91 ± 1.80
	ORCU (Ours)		0.5214 ± 0.0065	0.5199 ± 0.0067	0.0946 ± 0.0274	100.0 ± 0.00	0.5165 ± 0.0064	0.5139 ± 0.0070	0.0717 ± 0.0209	100.0 ± 0.00
Diabetic Retinopathy ($n=9,570$)										
	CE (Baseline)		0.6894 ± 0.0105	0.6857 ± 0.0094	0.2056 ± 0.0278	92.87 ± 0.95	0.7146 ± 0.0056	0.7118 ± 0.0063	0.2505 ± 0.0213	90.75 ± 1.35
Calibration-focused Ordinal-focused	SORD (Diaz & Marathe, 2019)		<u>0.6136 ± 0.0018</u>	<u>0.6124 ± 0.0018</u>	<u>0.0538 ± 0.0038</u>	<u>99.92 ± 0.05</u>	<u>0.6244 ± 0.0020</u>	<u>0.6236 ± 0.0025</u>	0.0354 ± 0.0100	<u>99.88 ± 0.04</u>
	CDW-CE (Polat et al., 2022a)		0.6811 ± 0.0182	0.6787 ± 0.0168	0.2474 ± 0.0256	99.44 ± 0.69	0.6991 ± 0.0060	0.6940 ± 0.0054	0.2132 ± 0.0198	<u>99.97 ± 0.05</u>
	CO2 (Albuquerque et al., 2021)		0.7152 ± 0.0103	0.7109 ± 0.0107	0.2761 ± 0.0152	88.86 ± 1.99	0.7314 ± 0.0075	0.7265 ± 0.0071	0.2839 ± 0.0190	88.03 ± 1.99
	POE (Li et al., 2021)		0.6790 ± 0.0077	0.6739 ± 0.0075	0.1699 ± 0.0222	89.18 ± 1.36	0.7028 ± 0.0045	0.6993 ± 0.0042	0.2115 ± 0.0089	91.03 ± 2.43
	LS (Szegedy et al., 2016)		0.6755 ± 0.0034	0.6720 ± 0.0035	0.1704 ± 0.0115	81.36 ± 0.95	0.6804 ± 0.0028	0.6763 ± 0.0021	0.1649 ± 0.0109	78.37 ± 0.73
	FLSD (Mukhoti et al., 2020)		0.6543 ± 0.0069	0.6533 ± 0.0071	0.1200 ± 0.0131	94.52 ± 1.18	0.6888 ± 0.0100	0.6855 ± 0.0103	0.1752 ± 0.0204	93.30 ± 1.11
	MbLS (Liu et al., 2022)		0.6896 ± 0.0069	0.6858 ± 0.0076	0.2080 ± 0.0186	87.21 ± 0.80	0.7104 ± 0.0035	0.7070 ± 0.0026	0.2290 ± 0.0119	83.94 ± 0.96
	MDCA (Hebbalaguppe et al., 2022)		0.6857 ± 0.0102	0.6821 ± 0.0101	0.1927 ± 0.0211	92.92 ± 0.94	0.7055 ± 0.0053	0.7019 ± 0.0050	0.2187 ± 0.0146	92.11 ± 1.36
	ACLS (Park et al., 2023)		0.6920 ± 0.0051	0.6893 ± 0.0045	0.2145 ± 0.0160	87.78 ± 1.32	0.7100 ± 0.0033	0.7063 ± 0.0038	0.2379 ± 0.0152	84.34 ± 1.52
	ORCU (Ours)		0.5427 ± 0.0163	0.5420 ± 0.0167	0.0410 ± 0.0043	99.98 ± 0.01	0.5444 ± 0.0068	0.5433 ± 0.0072	0.0413 ± 0.0039	99.99 ± 0.02

Table 3. Classification performance of \mathcal{L}_{ORCU} compared to baseline loss functions on four ordinal datasets. Metrics include Accuracy (Acc), Quadratic Weighted Kappa (QWK), and Mean Absolute Error (MAE). Results are presented as mean and standard deviation across folds. Bold values indicate the best performance and underlined values represent the second-best.

Loss	Dataset	Metrics	Image Aesthetics ($n=13,364$)			Adience ($n=17,423$)			LIMUC ($n=11,276$)			Diabetic Retinopathy ($n=9,570$)		
			Acc↑	QWK↑	MAE↓	Acc↑	QWK↑	MAE↓	Acc↑	QWK↑	MAE↓	Acc↑	QWK↑	MAE↓
	CE (Baseline)		0.7030 ± 0.0080	0.4961 ± 0.0199	0.3106 ± 0.0091	0.5639 ± 0.0486	0.8795 ± 0.0345	0.5504 ± 0.0704	0.7702 ± 0.0066	0.8461 ± 0.0090	0.2387 ± 0.0083	0.5411 ± 0.0115	0.7663 ± 0.0153	0.5940 ± 0.0223
Calibration-focused Ordinal-focused	SORD (Diaz & Marathe, 2019)		0.7092 ± 0.0044	<u>0.5030 ± 0.0030</u>	0.3002 ± 0.0031	0.5910 ± 0.0439	0.8995 ± 0.0291	0.4875 ± 0.0585	0.7749 ± 0.0060	0.8539 ± 0.0062	0.2314 ± 0.0063	0.5307 ± 0.0086	<u>0.7920 ± 0.0092</u>	0.5677 ± 0.0132
	CDW-CE (Polat et al., 2022a)		0.7041 ± 0.0064	0.4837 ± 0.0148	0.3062 ± 0.0063	0.5789 ± 0.0362	0.8988 ± 0.0257	0.4948 ± 0.0486	0.7773 ± 0.0058	0.8551 ± 0.0069	0.2288 ± 0.0067	0.5347 ± 0.0114	0.7968 ± 0.0081	0.5562 ± 0.0144
	CO2 (Albuquerque et al., 2021)		0.6980 ± 0.0072	0.4919 ± 0.0158	0.3155 ± 0.0066	0.5637 ± 0.0489	0.8728 ± 0.0073	0.5604 ± 0.0765	0.7662 ± 0.0076	0.8411 ± 0.0081	0.2432 ± 0.0086	0.5390 ± 0.0065	0.7678 ± 0.0104	0.5881 ± 0.0115
	POE (Li et al., 2021)		0.7015 ± 0.0058	0.4854 ± 0.0150	0.3148 ± 0.0075	0.5729 ± 0.0447	0.8755 ± 0.0304	0.5473 ± 0.0603	0.7660 ± 0.0074	0.8392 ± 0.0111	0.2449 ± 0.0100	0.5446 ± 0.0061	0.7678 ± 0.0104	0.5873 ± 0.0095
	LS (Szegedy et al., 2016)		0.7063 ± 0.0054	0.4990 ± 0.0122	0.3063 ± 0.0011	0.5792 ± 0.0495	0.8824 ± 0.0371	0.5300 ± 0.0739	0.7633 ± 0.0055	0.8402 ± 0.0086	0.2467 ± 0.0067	0.5466 ± 0.0126	0.7655 ± 0.0172	0.5897 ± 0.0236
	FLSD (Mukhoti et al., 2020)		0.7015 ± 0.0059	0.4992 ± 0.0145	0.3111 ± 0.0057	0.5718 ± 0.0508	0.8804 ± 0.0344	0.5415 ± 0.0726	0.7740 ± 0.0055	0.8493 ± 0.0077	0.2347 ± 0.0072	0.5458 ± 0.0090	0.7655 ± 0.0172	0.5796 ± 0.0116
	MbLS (Liu et al., 2022)		0.7040 ± 0.0057	0.4942 ± 0.0159	0.3102 ± 0.0063	0.5794 ± 0.0467	0.8825 ± 0.0324	0.5291 ± 0.0639	0.7655 ± 0.0079	0.8409 ± 0.0081	0.2449 ± 0.0087	<u>0.5473 ± 0.0080</u>	0.7700 ± 0.0141	0.5848 ± 0.0193
	MDCA (Hebbalaguppe et al., 2022)		0.7030 ± 0.0057	0.4993 ± 0.0129	0.3110 ± 0.0053	0.5618 ± 0.0527	0.8778 ± 0.0364	0.5538 ± 0.0740	0.7692 ± 0.0048	0.8413 ± 0.0060	0.2415 ± 0.0049	0.5499 ± 0.0083	0.7739 ± 0.0142	0.5800 ± 0.0163
	ACLS (Park et al., 2023)		0.7031 ± 0.0075	0.4953 ± 0.0147	0.3102 ± 0.0071	0.5762 ± 0.0488	0.8788 ± 0.0366	0.5383 ± 0.0704	0.7683 ± 0.0089	0.8454 ± 0.0092	0.2407 ± 0.0099	0.5410 ± 0.0048	0.7708 ± 0.0141	0.5893 ± 0.0142
	ORCU (Ours)		0.7074 ± 0.0064	0.5152 ± 0.0113	<u>0.3027 ± 0.0053</u>	0.5750 ± 0.0427	0.8974 ± 0.0299	0.5071 ± 0.0603	0.7838 ± 0.0073	0.8621				

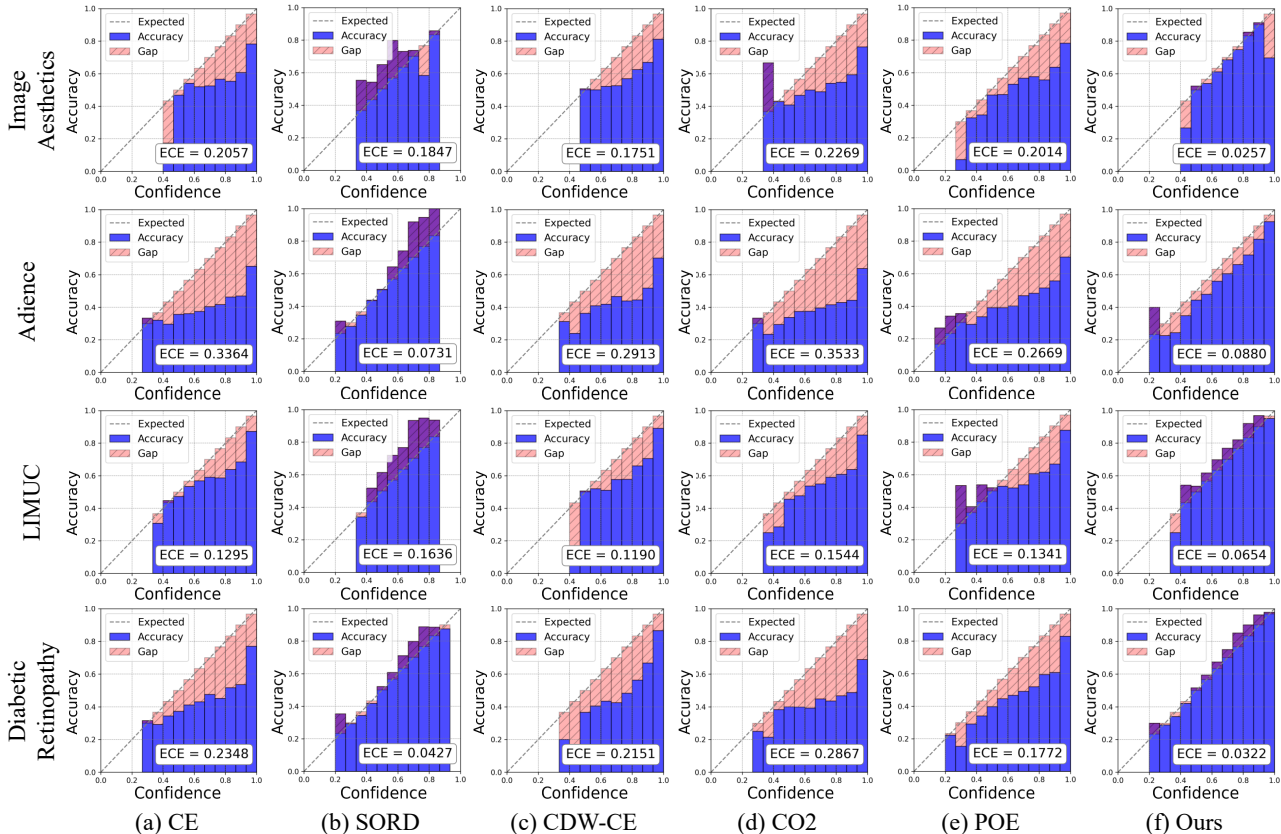


Figure 2. Reliability diagrams comparing ordinal loss functions on the test splits of Image Aesthetics, Adience, LIMUC, and Diabetic Retinopathy. The diagrams show the calibration gap between model confidence and accuracy. Bars above the expected line indicate underconfidence ($P(Y = y | \hat{P} = p) > p$), while those below indicate overconfidence ($P(Y = y | \hat{P} = p) < p$). ECE is computed using 15 bins.

D.3. Visual Analyses

D.3.1. RELIABILITY DIAGRAMS

Figure 2 and Figure 3 provide reliability diagrams comparing \mathcal{L}_{ORCU} with ordinal-focused and calibration-focused loss functions, respectively. CE-based approaches (Figure 2-(a), (c)-(e)) consistently exhibit overconfidence, with predictions frequently exceeding the expected calibration line. SORD (Figure 2-(b)), designed to align predictions with a soft-encoded distribution instead of a one-hot target, captures ordinal relationships through a dispersed label distribution. However, this approach limits predictions to a restricted confidence range, making it challenging to achieve reliable calibration. In contrast, the proposed \mathcal{L}_{ORCU} overcomes these limitations (Figure 2-(f)) by addressing SORD’s underconfidence and extending reliability to high-confidence predictions, resulting in more dependable confidence estimates.

Calibration-focused loss functions, while intended to improve calibration, often fail in ordinal tasks due to their inability to account for ordinal relationships (Figure 3-(b)-(e)). As a result, most of these methods show limited calibration improvements and frequently display severe overconfidence, similar to the baseline CE. LS, among these, achieves relatively better ECE performance, as illustrated in the reliability diagrams (Figure 3-(a)). However, its lack of ordinal awareness undermines its effectiveness in ordinal tasks, as will be further explored in the softmax output analysis (Figure 6). These results confirm the effectiveness of \mathcal{L}_{ORCU} in leveraging ordinal relationships to achieve superior calibration in ordinal tasks.

D.3.2. T-SNE VISUALIZATIONS

Figure 4 provides a comparison of t-SNE visualizations for models trained with \mathcal{L}_{ORCU} and baseline loss functions on the Adience, LIMUC, and Diabetic Retinopathy datasets. The Image Aesthetics dataset is excluded from this analysis

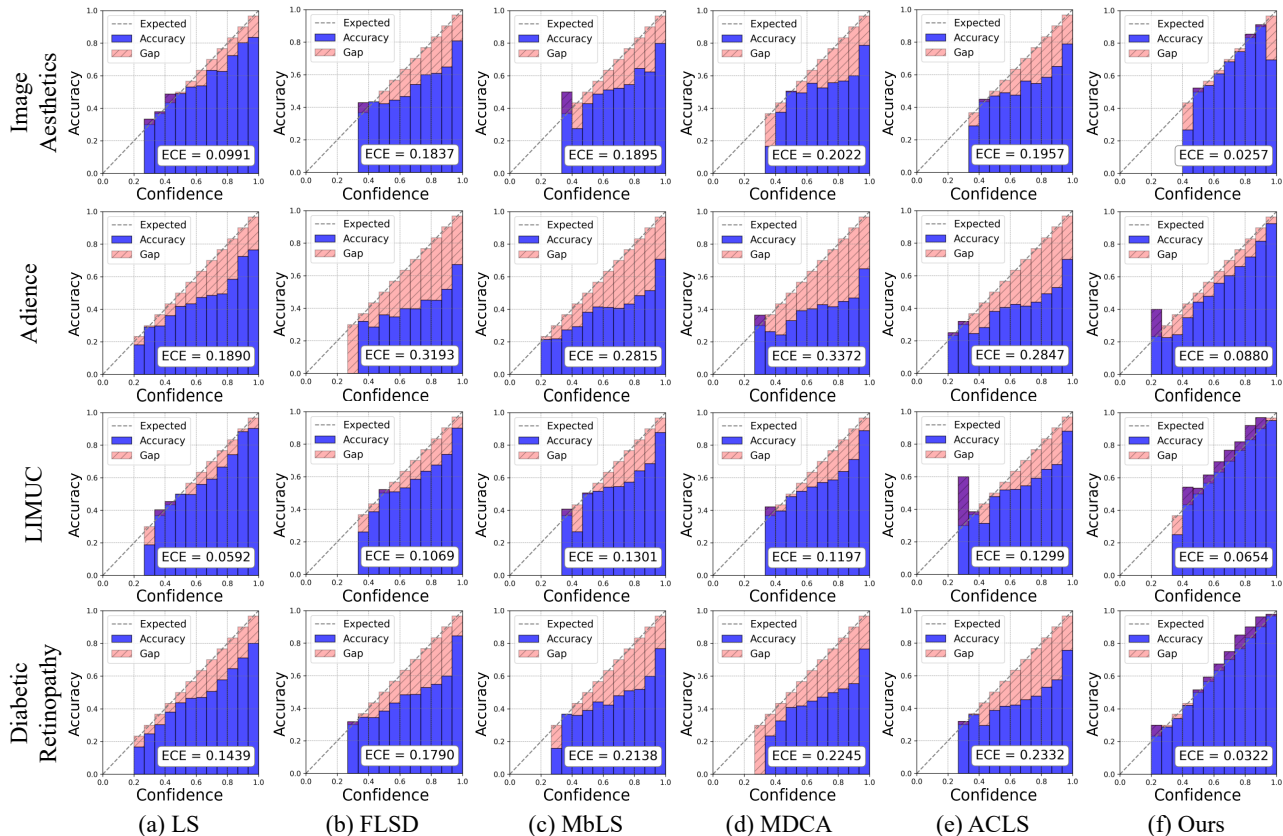


Figure 3. Reliability diagrams comparing calibration loss functions on the test splits of Image Aesthetics, Adience, LIMUC, and Diabetic Retinopathy. The diagrams show the calibration gap between model confidence and accuracy. Bars above the expected line indicate underconfidence ($P(Y = y | \hat{P} = p) > p$), while those below indicate overconfidence ($P(Y = y | \hat{P} = p) < p$). ECE is computed using 15 bins.

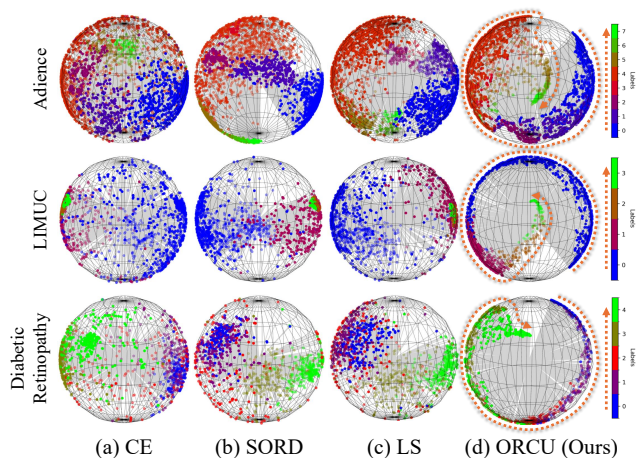


Figure 4. t-SNE visualizations of feature embeddings from the penultimate layer of ResNet-50 trained on the Adience, LIMUC, and Diabetic Retinopathy datasets. The plots illustrate the ability of each method to capture ordinal relationships, with colors representing class label order. The orange dashed line shows feature alignment, demonstrating effective ordinal learning.

due to its highly imbalanced class distribution, which makes embedding comparisons through t-SNE challenging. \mathcal{L}_{ORCU} (Figure 4-(d)) generates embeddings that are relatively well-aligned with label order compared to other loss functions. The

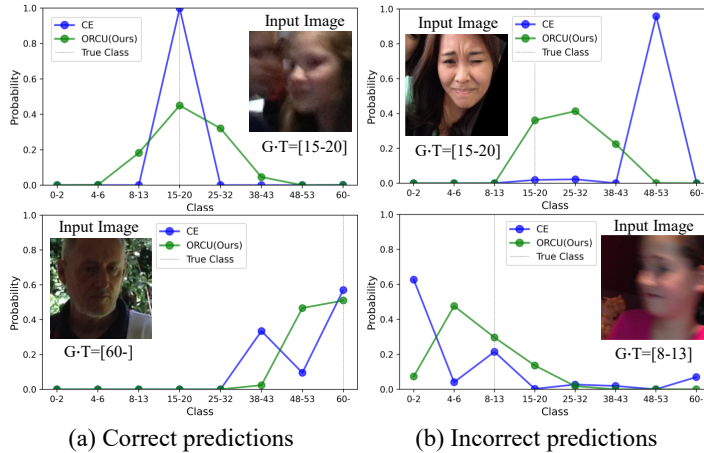


Figure 5. Output distributions of models trained with CE and ORCU on the Adience test split, showing (a) correct and (b) incorrect predictions. Each subfigure compares ORCU (green) with CE (blue), with the gray dashed line representing the ground-truth age group.

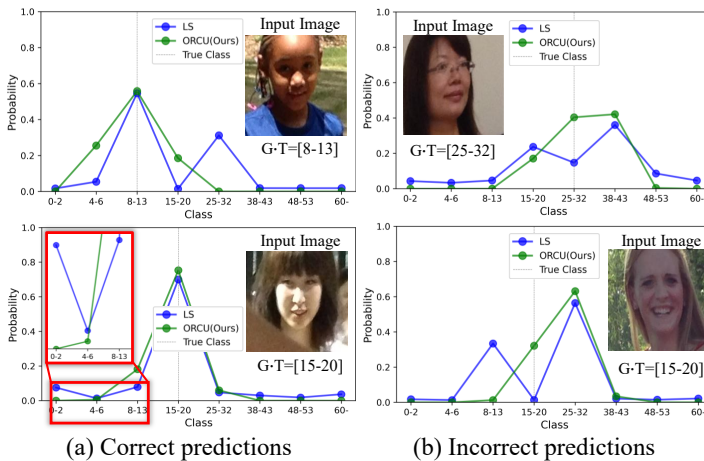


Figure 6. Output distributions of models trained with LS and ORCU on the Adience test split, showing (a) correct and (b) incorrect predictions. Each subfigure compares ORCU (green) with SORD (blue), with the gray dashed line representing the ground-truth age group.

comparison with SORD (Figure 4-(b)) illustrates the influence of the regularization term that operates based on label order. These label-order-aligned feature embeddings suggest that models trained with \mathcal{L}_{ORCU} may effectively utilize inherent label relationships to make predictions.

D.3.3. SOFTMAX OUTPUT DISTRIBUTION

Figure 5 compares the softmax output distributions of models trained with CE and \mathcal{L}_{ORCU} on the Adience dataset. For correct predictions (Figure 5-(a)), models trained with CE produce overly confident outputs, regardless of input-specific uncertainty. In contrast, models trained with \mathcal{L}_{ORCU} exhibit calibrated predictions that adjust confidence levels based on input uncertainty, providing more conservative estimates for uncertain inputs. For incorrect predictions (Figure 5-(b)), CE assigns disproportionately high confidence to a single incorrect label, neglecting ordinal relationships. Conversely, models trained with \mathcal{L}_{ORCU} distribute confidence across adjacent labels, maintaining ordinal consistency and adequately reflecting uncertainty. In both cases, CE’s reliance on one-hot encoding results in poor alignment with inherent ordinal relationships. By integrating ordinal relationships during training, \mathcal{L}_{ORCU} facilitates consistent and reasonable predictions that align with the natural order of labels.

Figure 6 compares the softmax output distributions of models trained with LS and \mathcal{L}_{ORCU} on the Adience dataset. LS shows relatively strong calibration performance as measured by the ECE metric, outperforming other calibration-focused

losses. However, it lacks consistency in preserving ordinal relationships, which is essential for ordinal classification. For correct predictions (Figure 6-(a)), models trained with LS and $\mathcal{L}_{\text{ORCU}}$ provide similar confidence estimates for the target label. However, LS predictions violate unimodality, resulting in order-inconsistent outputs. For incorrect samples (Figure 6-(b)), models trained with LS produce predictions misaligned with the requirements of ordinal tasks due to the absence of an order-awareness mechanism. In contrast, $\mathcal{L}_{\text{ORCU}}$ maintains balanced confidence distributions across adjacent likely labels, preserving order-aware unimodality and reflecting input-specific uncertainty. These findings demonstrate $\mathcal{L}_{\text{ORCU}}$'s effectiveness in delivering reliable confidence estimates while capturing ordinal structure.

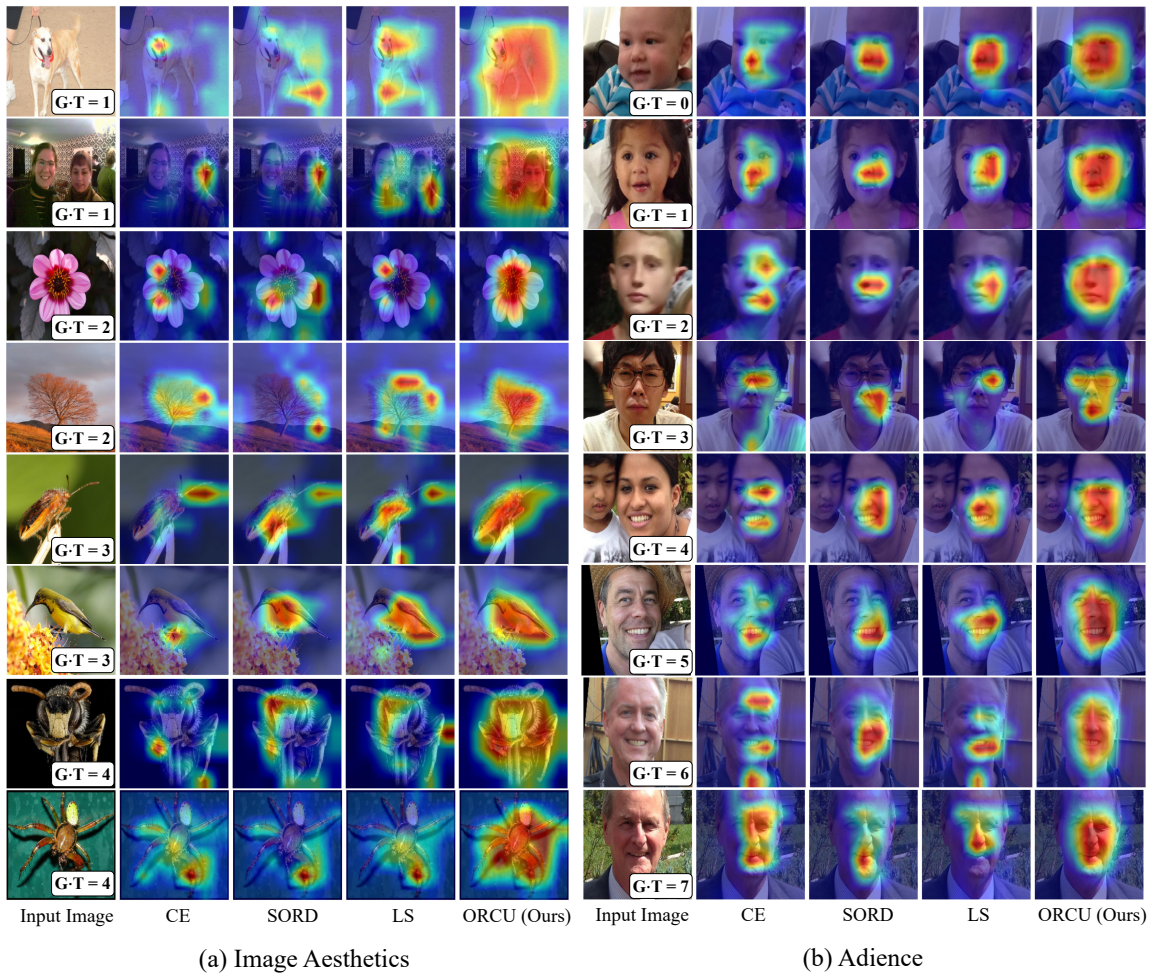


Figure 7. Grad-CAM visualizations from the final convolutional layer of ResNet-50 trained with CE, SORD, LS, and $\mathcal{L}_{\text{ORCU}}$ on (a) Image Aesthetics and (b) Adience datasets, representing a general computer vision context. Activation maps indicate regions contributing to model predictions, with colors showing activation intensity (red: high, blue: low). Visualizations are derived from correctly predicted samples.

D.3.4. GRAD-CAM VISUALIZATIONS

Figure 7 presents Grad-CAM activation maps (Gildenblat & contributors, 2021) for models trained with CE, SORD, LS, and ORCU on the Image Aesthetics and Adience datasets. These datasets are selected as they represent general computer vision tasks, enabling qualitative evaluation of feature localization. These visualizations, generated from correctly predicted samples, reveal notable differences in feature localization across the various loss functions. Models trained with ORCU consistently generate broader activation maps compared to those trained with other loss functions. Particularly, compared to SORD, ORCU integrates an ordinal-aware regularization term that enhances calibration and ordinal consistency by leveraging the inherent relationships among labels, resulting in superior feature representation quality and improved interpretability (Suara et al., 2023; Tan et al., 2024) in ordinal classification tasks.

Table 4. Full table of ablation studies on the choice of \mathcal{L}_{REG} and distance metrics used in \mathcal{L}_{SCE} , providing detailed results for $\mathcal{L}_{\text{ORCU}}$ and competing regularization methods ($\mathcal{L}_{\text{MbLS}}$, $\mathcal{L}_{\text{MDCA}}$, and $\mathcal{L}_{\text{ACLS}}$). The first row for each dataset corresponds to \mathcal{L}_{SCE} (Squared) as in SORD. Metrics include Static Calibration Error (SCE), Adaptive Calibration Error (ACE), Expected Calibration Error (ECE), and %Unimodality (%Unimodal). Symbol " denotes configurations that remain unchanged from the previous setting.

Combination		Metric	SCE↓	ACE↓	ECE↓	%Unimodal↑
$\mathcal{L}_{\text{SCE}(\phi=\{\})}$		$\mathcal{L}_{\{\}}_{\text{REG}}$	Image Aesthetics ($n=13,364$)			
Squared	+	-	0.6844 ± 0.0018	0.6833 ± 0.0018	0.1846 ± 0.0026	100.0 ± 0.00
"	+	MbLS	0.6866 ± 0.0021	0.6852 ± 0.0023	0.1921 ± 0.0057	100.0 ± 0.00
"	+	MDCA	0.6867 ± 0.0033	0.6859 ± 0.0035	0.1501 ± 0.0080	100.0 ± 0.00
"	+	ACLS	0.6836 ± 0.0028	0.6819 ± 0.0033	0.1829 ± 0.0081	100.0 ± 0.00
"	+	ORCU(Ours)	0.6447 ± 0.0022	0.6419 ± 0.0019	0.0257 ± 0.0040	100.0 ± 0.00
Absolute	+	"	0.6919 ± 0.0032	0.6883 ± 0.00330	0.0329 ± 0.0090	100.0 ± 0.00
Huber	+	"	0.6404 ± 0.0029	0.6847 ± 0.0028	0.0618 ± 0.0060	100.0 ± 0.00
Exponential	+	"	0.6856 ± 0.0017	0.6838 ± 0.0014	0.0965 ± 0.0105	99.99 ± 0.01
$\mathcal{L}_{\text{SCE}(\phi=\{\})}$		$\mathcal{L}_{\{\}}_{\text{REG}}$	Adience ($n=17,423$)			
Squared	+	-	0.7823 ± 0.0105	0.7783 ± 0.0102	0.0731 ± 0.0240	98.76 ± 0.95
"	+	MbLS	0.7823 ± 0.0092	0.7788 ± 0.0092	0.0711 ± 0.0217	92.12 ± 1.41
"	+	MDCA	0.7849 ± 0.0091	0.7810 ± 0.0100	0.0677 ± 0.0315	97.71 ± 0.89
"	+	ACLS	0.7827 ± 0.0099	0.7791 ± 0.0100	0.0746 ± 0.0239	92.04 ± 1.80
"	+	ORCU(Ours)	0.4193 ± 0.0218	0.4148 ± 0.0212	0.0880 ± 0.0227	99.94 ± 0.04
Absolute	+	"	0.7024 ± 0.0120	0.6985 ± 0.0108	0.0681 ± 0.0185	99.98 ± 0.02
Huber	+	"	0.7117 ± 0.0109	0.7086 ± 0.0100	0.0461 ± 0.0145	99.99 ± 0.01
Exponential	+	"	0.7840 ± 0.0109	0.7808 ± 0.0103	0.0551 ± 0.0341	99.97 ± 0.01
$\mathcal{L}_{\text{SCE}(\phi=\{\})}$		$\mathcal{L}_{\{\}}_{\text{REG}}$	LIMUC ($n=11,276$)			
Squared	+	-	0.6382 ± 0.0031	0.6370 ± 0.0032	0.1636 ± 0.0064	100.0 ± 0.00
"	+	MbLS	0.6398 ± 0.0026	0.6386 ± 0.0026	0.1662 ± 0.0056	100.0 ± 0.00
"	+	MDCA	0.6387 ± 0.0026	0.6368 ± 0.0027	0.1373 ± 0.0065	100.0 ± 0.00
"	+	ACLS	0.6366 ± 0.0029	0.6349 ± 0.0030	0.1590 ± 0.0067	100.0 ± 0.00
"	+	ORCU(Ours)	0.5133 ± 0.0056	0.5105 ± 0.0062	0.0654 ± 0.0073	100.0 ± 0.00
Absolute	+	"	0.6421 ± 0.0021	0.6381 ± 0.0021	0.0635 ± 0.0128	100.0 ± 0.00
Huber	+	"	0.6404 ± 0.0029	0.6364 ± 0.0038	0.1122 ± 0.0137	100.0 ± 0.00
Exponential	+	"	0.6388 ± 0.0027	0.6372 ± 0.0030	0.1524 ± 0.0130	99.99 ± 0.01
$\mathcal{L}_{\text{SCE}(\phi=\{\})}$		$\mathcal{L}_{\{\}}_{\text{REG}}$	Diabetic Retinopathy ($n=9,570$)			
Squared	+	-	0.6204 ± 0.0026	0.6196 ± 0.0023	0.0427 ± 0.0023	99.90 ± 0.04
"	+	MbLS	0.6208 ± 0.0031	0.6200 ± 0.0036	0.0465 ± 0.0066	99.27 ± 0.18
"	+	MDCA	0.6221 ± 0.0021	0.6210 ± 0.0008	0.0471 ± 0.0108	99.93 ± 0.02
"	+	ACLS	0.6199 ± 0.0031	0.6198 ± 0.0035	0.0507 ± 0.0110	99.43 ± 0.17
"	+	ORCU(Ours)	0.5471 ± 0.0126	0.5463 ± 0.0131	0.0322 ± 0.0080	99.96 ± 0.02
Absolute	+	"	0.6266 ± 0.0061	0.6253 ± 0.0064	0.0400 ± 0.0038	99.98 ± 0.02
Huber	+	"	0.6222 ± 0.0042	0.6217 ± 0.0047	0.0457 ± 0.0128	99.98 ± 0.01
Exponential	+	"	0.6201 ± 0.0022	0.6187 ± 0.0018	0.0668 ± 0.0174	99.98 ± 0.01

D.4. Comprehensive Ablation Study

Table 4 presents a comprehensive ablation study conducted on the Adience, Image Aesthetics, and LIMUC datasets, analyzing the effects of various regularization terms and distance metrics in \mathcal{L}_{SCE} . The results demonstrate that conventional calibration regularization terms are insufficient for achieving both effective calibration and unimodality, revealing their limitations in addressing the unique challenges of ordinal tasks. In contrast, combining the Squared distance metric with the proposed ordinal-aware regularization term consistently achieves robust calibration performance and ordinal alignment across datasets. This study provides a detailed evaluation of the key components essential for jointly learning calibration and ordinal structure in classification tasks.